Inorganic Chemistry

Forum Article

pubs.acs.org/IC

Lanthanide-Based Imaging of Protein−Protein Interactions in Live Cells

Megha Rajendran, Engin Yapici, and Lawrence W. Miller*

Department of Chemistry, University of Illinois at Chicago, 845 West Taylor Street, Chicago, Illinois 60607, United States

ABSTRACT: In order to deduce the molecular mechanisms of biological function, it is necessary to monitor changes in the subcellular location, activation, and interaction of proteins within living cells in real time. Förster resonance energy-transfer (FRET)-based biosensors that incorporate genetically encoded, fluorescent proteins permit high spatial resolution imaging of protein−protein interactions or protein conformational dynamics. However, a nonspecific fluorescence background often obscures small FRET signal changes, and intensity-based biosensor measurements require careful interpretation and several control experiments. These problems can be overcome by using lanthanide [Tb(III) or Eu(III)] complexes as donors and green fluorescent protein (GFP) or other conventional fluorophores as acceptors. Essential features of this approach are the long-lifetime (approximately milliseconds) luminescence of Tb(III) complexes and time-gated luminescence microscopy. This allows pulsed excitation, followed by a brief delay, which eliminates nonspecific fluorescence before the detection of Tb(III)-to-GFP emission. The challenges of intracellular delivery, selective protein labeling, and time-gated imaging of lanthanide luminescence are presented, and recent efforts to investigate the cellular uptake of lanthanide probes are reviewed. Data are presented showing that conjugation to arginine-rich, cell-penetrating peptides (CPPs) can be used as a general strategy for the cellular delivery of membrane-impermeable lanthanide complexes. A heterodimer of a luminescent Tb(III) complex, Lumi4, linked to trimethoprim and conjugated to nonaarginine via a reducible disulfide linker rapidly (∼10 min) translocates into the cytoplasm of Maden Darby canine kidney cells from the culture medium. With this reagent, the intracellular interaction between GFP fused to FK506 binding protein 12 (GFP−FKBP12) and the rapamycin binding domain of mTOR fused to *Escherichia coli* dihydrofolate reductase (FRB-eDHFR) were imaged at high signal-to-noise ratio with fast (1−3 s) image acquisition using a time-gated luminescence microscope. The data reviewed and presented here show that lanthanide biosensors enable fast, sensitive, and technically simple imaging of protein−protein interactions in live cells.

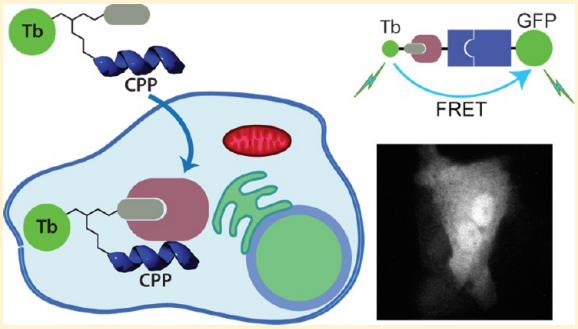

INTRODUCTION

Ligand-sensitized complexes of lanthanide cations, especially Tb(III) and Eu(III), have unique photophysical properties that make them particularly advantageous for luminescence-based biological analyses.[1,2] Following near-UV (320−400 nm) ligand absorption, Tb(III) and Eu(III) complexes emit at multiple, discrete wavelengths with narrow bandwidths (<10 nm at half-maximum) that span the visible and near-IR (NIR) spectral regions (Figure 1a). Most notably, emission lifetimes are long (0.1−2 ms), and this allows for time-gated detection (TGD) strategies, where pulsed light is used to excite the sample, and lanthanide emission is detected after a brief delay (approximately microseconds), which effectively eliminates scattering and short-lifetime (approximately nanoseconds) fluorescence background signals. The ability to temporally and spectrally isolate lanthanide emission signals makes it possible to detect analytes at small concentrations (picomolar to nanomolar) in complex matrixes, and lanthanide-based assays are routinely used for diagnostics and high-throughput screening using commercial-plate-reader instrumentation.[3,4] In recent years, there has been considerable interest in leveraging the inherent sensitivity of TGD with Tb(III) and Eu(III) complexes for applications in live-cell microscopic imaging.[1,2] In this context, the chemistry and photophysics of lanthanide complexes must be considered in relation to the workings and limitations of microscopes, the interaction and compatibility of complexes with cells, and the nature of the biological questions that are typically addressed by live-cell imaging experiments.

The photophysics and critical design features of luminescent lanthanide complexes are well established and have been amply described in many reviews.[5−7] Because lanthanide f−f transitions are parity-forbidden, direct excitation is inefficient, and emissive lanthanide complexes incorporate the metal ion into an organic chelating ligand that contains a sensitizing chromophore with a small singlet−triplet energy gap and a triplet energy at least 1500 cm^{-1} above the receiving Ln(III) level (Figure 1b).[7−9] Following light absorption by the chromophore, energy is transferred to the lanthanide excited state, which then emits. Most commonly, energy transfer

Special Issue: Imaging and Sensing

Received: July 19, 2013
Published: October 21, 2013

   dx.doi.org/10.1021/ic4018739 | *Inorg. Chem.* 2014, 53, 1839−1853

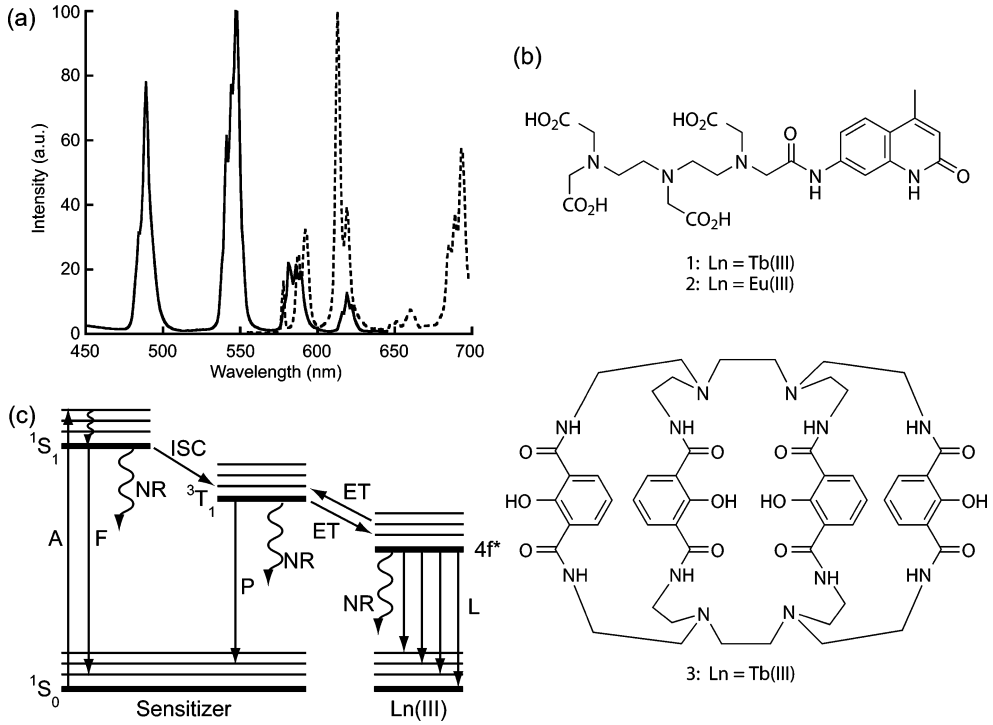

Figure 1. Structure and photophysics of sensitized organic lanthanide complexes. (a) Typical emission spectra of luminescent Tb(III) (solid) and Eu(III) (dotted) complexes. (b) Exemplary structures of sensitized lanthanide complexes. With DTPA-cs124, the chelator and sensitizer are separate entities.[8] The 7-amino-4-methyl-2(1*H*)-quinolinone (cs124) moiety effectively sensitizes both Tb(III) (**1**) and Eu(III) (**2**) luminescence. With the Lumi4-Tb(III) complex (**3**), the four hydroxyisophthalamide units serve as both chelators and sensitizers.[9] (c) Schematic representation of major energy transitions in a lanthanide complex. S = singlet state, T = triplet state, A = absorption, F = fluorescence, P = phosphorescence, NR = nonradiative, ISC = intersystem crossing, ET = energy transfer, and L = metal luminescence.

proceeds through the ligand triplet state, although transfer through singlet and charge-transfer states has been observed (Figure 1c). For practical use in bioassays, lanthanide complexes require several features: (i) kinetic inertness with respect to metal binding; (ii) a high extinction coefficient (>10000 M^{-1} cm^{-1}) and quantum yield (>0.1) of emission (i.e., good brightness); (iii) a long-wavelength (>350 nm) ligand absorption maximum; (iv) resistance to photobleaching; (v) one or more functional groups that can be used for conjugation to biomolecules or targeting moieties.[10] While hundreds of luminescent Tb(III) and Eu(III) complexes have been reported, relatively few meet all of the above-mentioned requirements.

For use in live-cell imaging, lanthanide complexes with long-wavelength absorption and good brightness are especially critical. Fluorescence microscopes incorporate high numerical aperture (NA) and aberration-corrected objectives to both deliver excitation light and collect emission signals. Very few of these objectives transmit light at wavelengths below 350 nm. Moreover, the resolution and signal-to-noise ratio (SNR) in optical imaging fundamentally depend on the number of photons collected. With millisecond-scale lifetimes, lanthanides have low photon emission rates (<1000 photons/s). Thus, the brightest possible lanthanide complexes must be used to allow for adequate photon collection within limited exposure times, as we discuss in more detail below.

Fluorescence microscopy is used most effectively to visualize dynamic changes in the concentration, location, interactions, or activity of biomolecules directly within the natural environment of the living cell. Central to this technique are luminescent markers: either sensing probes that report, say, localized changes in the analyte concentration (e.g., H_2O_2, Ca^{2+}, Zn^{2+})[11−13] or tags that bind selectively to specific proteins or other macromolecules.[14−16] The existing toolbox of organic fluorophores and genetically encoded fluorescent proteins currently enables multicolor fluorescence imaging in live cells with various millisecond time resolution, nanometer spatial precision, single-molecule sensitivity, and absolute biochemical specificity.[17,18] Given this context, it is worthwhile to consider the particular biological problems that can be addressed using lanthanide complexes and time-gated imaging that cannot be easily solved using existing technologies. In this Forum Article, we describe the use of lanthanide complexes as donors for time-gated Förster resonance energy transfer (FRET) microscopy with a particular focus on the imaging of protein−protein interactions in living mammalian cells. Time-gated microscopic technology is briefly reviewed and its technical aspects are presented in terms of quantitative measures of image quality including SNR, photon collection efficiency, and image acquisition time. Further, we attempt to define benchmark values of these parameters as they relate to obtaining high-quality images. We also emphasize, with examples from our group and others, experimental techniques to achieve controlled delivery of lanthanide labels and specific, intracellular labeling of proteins. While the focus is on FRET imaging of protein−protein interactions, the concepts and examples given here are also relevant for lanthanide-based FRET imaging of protein conformational dynamics as well as imaging of lanthanide complex-based sensors, another area of considerable research effort.[1,2,6]

dx.doi.org/10.1021/ic4018739 | *Inorg. Chem.* 2014, 53, 1839−1853

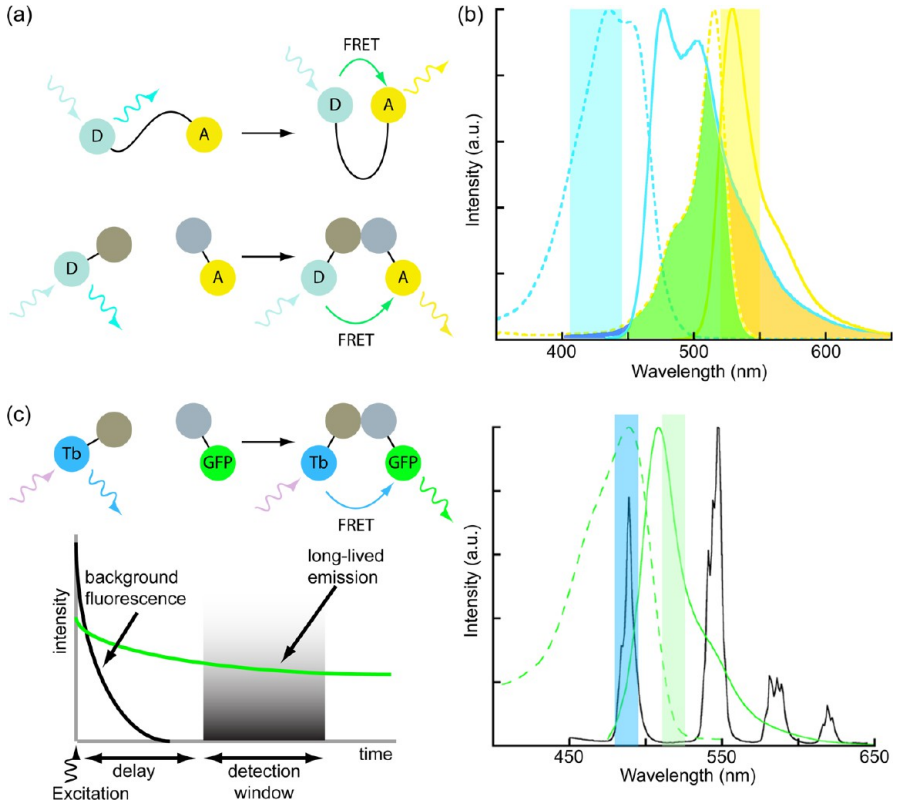

Figure 2. FRET-based biosensors and effects of donor and acceptor photophysics on detection. (a) Conformational changes of a single-chain biosensor (top) or interaction of dual-chain biosensor (bottom) components that bring donor (D) and acceptor (A) fluorophores within the FRET distance (<10 nm). (b) Excitation (dotted) and emission (solid) spectra of CFP (cyan) and YFP (yellow), a common donor−acceptor pair for live-cell FRET imaging. Overlap of CFP emission and YFP excitation spectra (green) allows sensitized YFP emission (yellow band) to be detected upon excitation of CFP (cyan band). Crosstalk, or direct excitation of YFP in the CFP band (blue) and bleedthrough of CFP emission into the YFP band (orange), obscures the true FRET signals, necessitating multiple measurements with different filter sets. (c) With a long-lifetime Tb(III) donor and short-lifetime GFP acceptor, Tb(III) and Tb(III)-sensitized GFP emission can be separated using narrow-pass emission filters, eliminating bleedthrough. Crosstalk is eliminated by TGD of long-lifetime Tb(III)-to-GFP FRET.

FRET IMAGING

In order to deduce the molecular mechanisms by which proteins regulate cellular processes such as signal transduction, it is necessary to monitor changes in both the subcellular location and protein activity in living cells in real time.[19] Often, changes in the protein activity are correlated with changes in the conformation or propensity to interact with other proteins. FRET microscopy has emerged as a powerful tool for dynamically imaging changes in the level of interaction between two proteins or in the conformation of a single protein.[20−22] FRET is the radiationless transfer of energy from an excited fluorescent donor to a nearby (<10 nm) acceptor whose absorption spectrum overlaps with the donor emission spectrum. FRET can be detected as a decrease in the fluorescence intensity, lifetime, or anisotropy of the donor or as an increase in the fluorescence intensity of the acceptor upon donor excitation (if the acceptor is fluorescent).[23] Because the energy-transfer efficiency inversely varies with the sixth power of the separation between the donor and acceptor, FRET signal changes are highly sensitive to distance changes over the length scale of proteins. FRET-based biosensors for live-cell imaging often incorporate two differently colored fluorescent proteins, usually cyan (cyan fluorescent protein, CFP) and yellow (yellow fluorescent protein, YFP) as donors and acceptors, to read out changes in the protein conformation or interaction (Figure 2a).[22,24]

FRET between two fluorescent proteins is usually imaged in one of three ways: (i) detection of donor-sensitized acceptor emission at steady state (so-called "filter FRET"); (ii) detection of donor dequenching upon acceptor photobleaching; (iii) detection of changes in the donor emission lifetime using fluorescence lifetime imaging microscopy (FLIM).[23,24] The practical challenge with any of these techniques is to differentiate biologically relevant FRET signal changes from other sources of fluorescence present in a live cell, and each method has various advantages and disadvantages. At this point in time, filter FRET is the most commonly used method, can be easily implemented on wide-field epifluorescence microscopes, and in certain circumstances can be used to measure the energy-transfer efficiency on a pixel-by-pixel basis in a whole-cell image.[24] The acceptor photobleaching method can be used to directly measure the FRET efficiency (the fraction of excited donors that transfer energy), but it can destroy the sample and precludes time-lapse studies.[23,24] Fluorescence lifetime imaging microscopy (FLIM) can measure FRET independently of changes in the fluorophore concentration or emission intensity across the sample. However, FRET−FLIM measurements in the time domain require expensive instrumentation, long (approximately minutes) image acquisition times, and complex data-fitting algorithms to resolve nanosecond-scale lifetimes.[25] Frequency-domain FRET−FLIM instruments that incorporate inexpensive light-emitting-diode (LED) light sources can achieve relatively fast (~10 s) frame rates.[26,27] Recently, the

dx.doi.org/10.1021/ic4018739 | Inorg. Chem. 2014, 53, 1839−1853

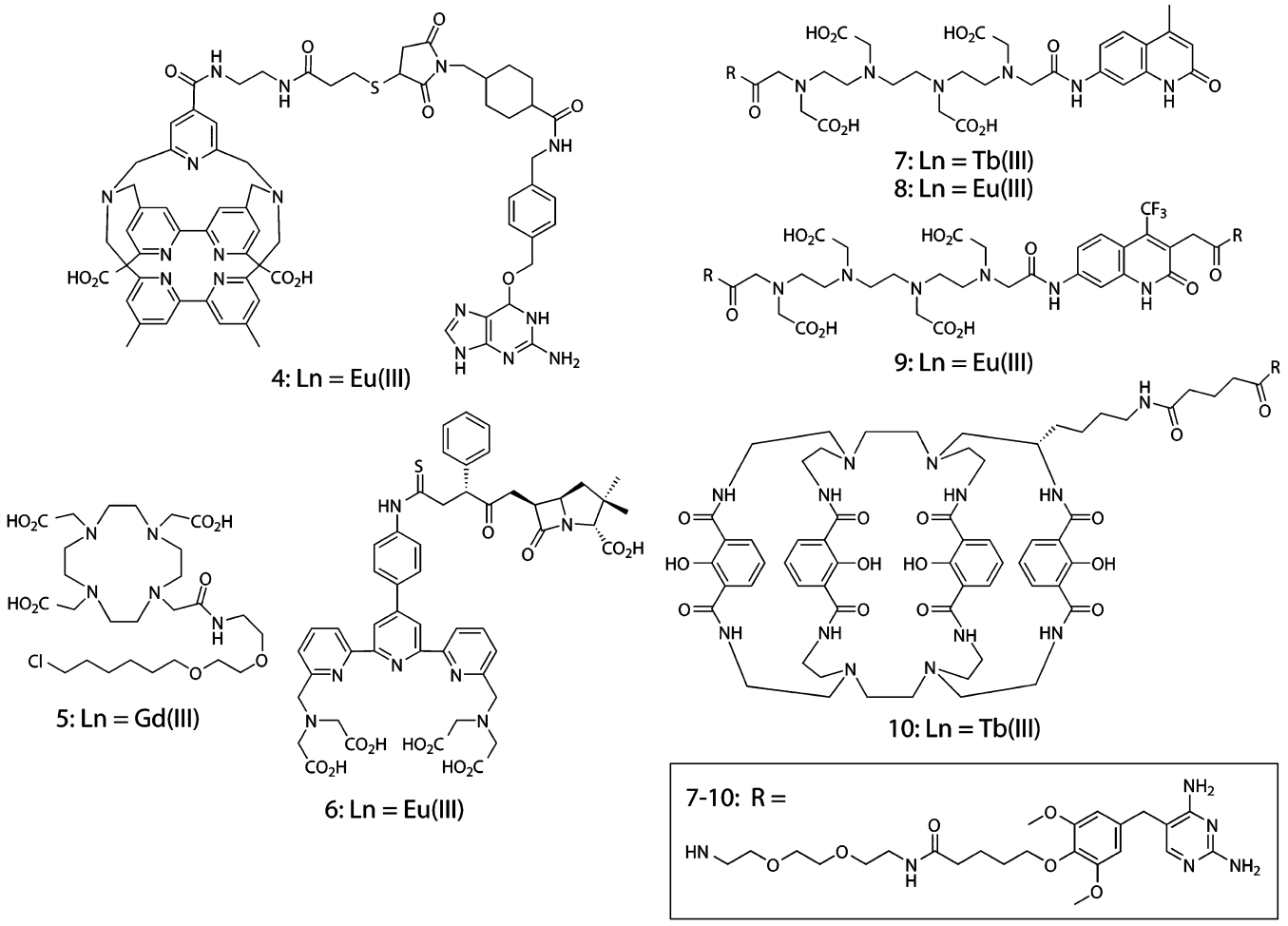

Figure 3. Ligand–lanthanide complex heterodimers that bind selectively to recombinant receptor fusion proteins in vitro or in live cells.

so-called phasor or polar plot methods of image analysis have been shown to accurately measure relative FRET changes without having to explicitly determine the lifetimes, thereby allowing for faster image acquisition.[28−30]

When used to image intermolecular interactions between two labeled proteins, i.e., when imaging a dual-chain biosensor, the filter FRET method is limited by (i) crosstalk (direct acceptor excitation by light used to excite the donor), (ii) bleedthrough (partial overlap of donor and acceptor emission wavelengths), and (iii) nonunitary ratios of donor- and acceptor-labeled proteins (Figure 2b).[23,24,31] Because of these limitations, at least three images must be collected with different filter sets: donor excitation/donor emission, donor excitation/acceptor emission (FRET), and acceptor excitation/acceptor emission. The images are then processed postacquisition to separate biochemically relevant FRET signals from non-FRET fluorescence background and to normalize the FRET signal to the amounts of donor and/or acceptor.[31] Even with these corrections, sensitized emission FRET suffers from low SNR, which often leads to false negative results (i.e., interaction occurs but is not seen) and can prevent accurate quantitative measurements.[24] When used to image conformational changes of a single-chain biosensor labeled with both donor and acceptor fluorophores, the image acquisition and processing requirements are less stringent, and two-color, ratiometric imaging (donor excitation/donor emission and donor excitation/acceptor emission) is often sufficient to quantify FRET signal changes.[31] The problems of crosstalk and bleedthrough are inherent to the broad excitation and emission spectra of fluorescent proteins, and they present an even greater challenge when one wishes to perform multiplexed imaging of two or more FRET biosensors in a single cell.[19,32]

The use of lanthanides, especially Tb(III), as FRET donors along with TGD (often referred to as lanthanide-based FRET, or LRET) offers distinct advantages over conventional FRET with fluorescent proteins for imaging molecular interactions in live cells.[5] First, bleedthrough is minimized because the narrow emission bands of Tb(III) can be spectrally isolated from sensitized acceptor emission signals (Figure 2c). Second, TGD eliminates directly excited acceptor fluorescence (crosstalk) and autofluorescence background signals. Thus, Tb(III)-sensitized emission of, for example, green fluorescent protein (GFP), can be detected in a single microscopic image by exciting Tb(III) with near-UV light and acquiring the GFP emission through a narrow-pass filter centered at 520 nm following a brief delay (approximately microseconds) after excitation (Figure 2c). A third benefit of Tb(III)-based FRET imaging is that it affords the possibility of multiplexed FRET imaging, where Tb(III) can sensitize emission of two or more differently colored acceptors.[33] Finally, it should be noted that time-gated imaging can be implemented on a conventional wide-field fluorescence microscope in a straightforward manner using commercially available components.[34] To fully implement time-gated FRET microscopy of protein–protein interactions, suitably bright and

dx.doi.org/10.1021/ic4018739 | Inorg. Chem. 2014, 53, 1839−1853

stable lanthanide complexes that can be selectively targeted to proteins in live cells, methods to deliver these complexes into specific cellular compartments without unduly perturbing cellular physiology,[2] and a time-gated luminescence microscope are required.

TIME-GATED LUMINESCENCE MICROSCOPY

The potential benefits of TGD for sensitive microscopic imaging of long-lived luminescence were first recognized in the early 1990s when epifluorescence microscopes equipped with a pulsed xenon flashlamp as the excitation source and chopper-gated charge-coupled detectors (CCDs) were used to image inorganic phosphors and europium chelates in immunohistochemical specimens.[35,36] Time-gated imaging of Tb(III) or Eu(III) luminescence requires pulsed UV excitation and the ability to turn on or unshutter the detector after the end of the excitation pulse. Various microscope configurations have been described that utilize flashlamps, pulsed lasers, or LEDs for excitation and mechanically or electronically gated CCDs.[37] Most of these systems employ through-objective sample illumination and wide-field array detection, although a time-gated, two-photon scanning microscope has been reported.[38] Multiphoton excitation of lanthanide complexes in the NIR could also be used to avoid potentially phototoxic UV illumination when imaging live cells, and some examples of two-photon imaging of lanthanide luminescence in cells have been reported.[39−41] However, the inherently low photon emission rates of lanthanide complexes require long pixel dwell times and therefore long image acquisition times.

In our laboratory, we adapted a conventional epifluorescence microscope for time-gated imaging by incorporating a collimated UV LED (365 nm) excitation source, an intensified CCD (ICCD) camera, and a pulse generator for synchronized triggering of the source and detector.[34] With this system, the intensifier component serves both as a shutter and as an emission signal amplifier, and the output of multiple excitation/emission cycles can be integrated on the CCD sensor during a single camera frame. The instrument is capable of rapidly (1−3 s) acquiring images of dim lanthanide specimens including 40 nm nanospheres [containing ∼400 Eu(III) complex molecules], Tb(III) complexes in the cytoplasm of living mammalian cells (cellular concentration 1−10 μM), and long-lifetime (20−200 μs), nonmetal luminescent probes.[42] The ability to quickly acquire high-contrast images from a minimal number of emitting molecules is critical for live-cell imaging because overly long exposure times increase the phototoxicity and limit temporal resolution. Under such imaging conditions, only a few tens of photons per pixel may be acquired from lanthanide emitters in a single camera frame. Therefore, the gain function of the intensifier is critical for producing images with adequate SNR.

PROTEIN-TARGETED LANTHANIDE COMPLEXES

Time-gated imaging studies require a reliable means to selectively and stably label a protein with a lanthanide complex. A variety of hybrid, chemical-genetic labeling methods have been developed that can be used to attach fluorophores or other functional small molecules to proteins in live cells.[14−16] These methods generally employ a strategy whereby target proteins are genetically encoded as fusions to a receptor protein, protein domain, or peptide sequence. The small-molecule probe consists of a receptor-binding ligand coupled to a fluorophore or other functional entity. Note that here the term "ligand" refers to the receptor-targeting moiety and not to a metal-complexing agent. Ideally, the ligand binds non-covalently or covalently to the recombinantly expressed, receptor protein fusion without appreciable nonspecific binding to other cellular targets. Ligand−receptor methods have been used in a few cases to label proteins with luminescent lanthanide species (Figure 3). Pin and co-workers covalently labeled g-protein-coupled receptors (GPCRs) with Eu(III) and Tb(III) complexes for time-gated FRET spectroscopic studies of GPCR oligomerization. Heterodimers of the macrocyclic Tb(III) complex, Lumi4-Tb, linked to O^6-benzylguanine and O^2-benzylcytosine and an O^6-benzylguanine Eu(III) cryptate analogue (**4**) were used to tag GPCR subunits fused to mutant forms of human alkylguanine alkyltransferase (SNAP-Tag and CLIP-Tag) on the surface of mammalian cells.[43,44] The Meade laboratory reported increased relaxivity of chloroalkyl-derivatized DOTA-Gd(III) magnetic resonance (MR) contrast agents such as **5** upon binding to an engineered dehalogenase protein (Halo-Tag) in vitro.[45] Mizukami et al. reported binding and time-gated luminescence imaging of **6**, an ampicillin−terpyridinetetracetateeuropium(III) conjugate to cell-surface TEM-1 β-lactamase.[46]

In our laboratory, we have leveraged the noncovalent interaction between the common antibiotic trimethoprim (TMP) and the *Escherichia coli* form of dihydrofolate reductase (eDHFR) to develop protein-targeted lanthanide labels. TMP binds tightly (K_D = ∼1 nM) to eDHFR but weakly (K_D > 1 μM) to mammalian forms of the enzyme, thereby allowing selective labeling of eDHFR fusion proteins in cultured mammalian cells or cell lysates.[47,48] Because eDHFR is small (∼18 kDa), soluble, and monomeric, it can be fused to the N- or C-terminus of target proteins with minimal perturbation of the native function. Conjugates of TMP linked to Tb(III) and Eu(III) poly(aminocarboxylate) complexes (**7**−**9**) and to the macrocyclic complex Lumi4-Tb (**10**) retain characteristic lanthanide luminescence and nanomolar affinity for eDHFR fusion proteins in purified preparations and in bacterial lysates.[49,50] Moreover, TMP-linked Tb(III) complexes are excellent FRET donors to GFP. In an in vitro assay performed in 96-well plates, we titrated a fusion of GFP to FK506 binding protein 12 (GFP−FKBP12) against a fixed concentration of eDHFR fused to the rapamycin binding domain of mTOR (FRB−eDHFR). Following the addition of rapamycin (to induce protein interaction) and the TMP-Tb(III) complex **7**, we observed a ∼3500% increase in the long-lifetime, Tb-to-GFP-sensitized emission.[51] The high dynamic range of Tb(III)-based FRET (>30-fold) greatly exceeds the best dynamic range for nondimerizing fluorescent proteins (<5-fold) observed in vitro and hints at the potential sensitivity of lanthanide-based FRET microscopy.[24,52]

IMAGING PROTEIN−PROTEIN INTERACTIONS: PROOF-OF-PRINCIPLE

We first demonstrated successful time-gated imaging of protein−protein interactions in living cells using a TMP−Lumi4 heterodimer (**10**).[53] As a model, we imaged the association of the most N-terminal PDZ domain of ZO-1 with the C-terminal binding motif of the transmembrane protein claudin-1. In epithelia, ZO-1 directs polymerization of claudins, which is necessary to form tight junctions,[54] and a direct interaction between ZO-1/PDZ-1 and the C-terminal cytoplasmic tail domain of claudin-1 has been demonstrated

dx.doi.org/10.1021/ic4018739 | Inorg. Chem. 2014, 53, 1839−1853

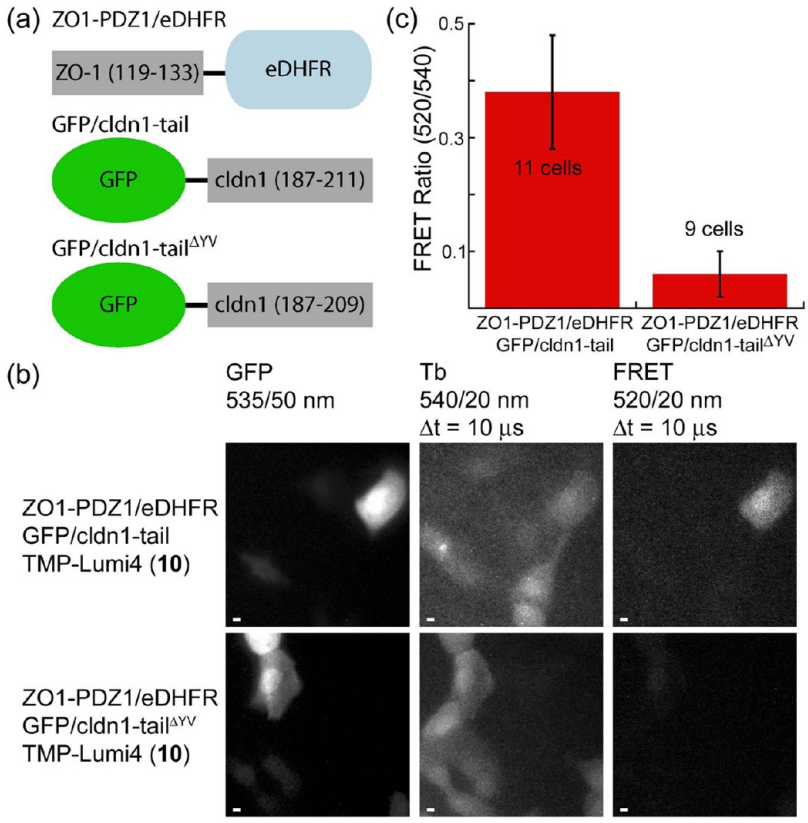

Figure 4. Time-gated FRET microscopy that detects protein−protein interactions in live cells with high confidence in single-frame images. (a) Schematic of fusion proteins. (b) MDCKII cells loaded with a TMP−Lumi4[Tb(III)] heterodimer (**10**) by osmotic lysis of pinosomes. Cells coexpressing indicated fusion proteins exhibited steady-state GFP fluorescence (left). TGD of Tb(III) luminescence (middle) revealed cells loaded with **10**. Tb(III)-to-GFP FRET (right) is seen in cells coexpressing ZO1-PDZ1/eDHFR and GFP/cldn1-tail and loaded with **10**. No FRET signal is visible in cells coexpressing noninteracting ZO1-PDZl/eDHFR and GFP/cldn1-tail$^{\Delta YV}$ and loaded with **10**. Micrographs: GFP fluorescence, λ_{ex} = 480/40 nm; time-gated luminescence, λ_{ex} = 365 nm, Δt = delay between excitation and detection. Emission at indicated wavelengths. Scale bar, 5 μm. (c) Significant ($P < 10^{-6}$) >500% difference in the mean, donor-normalized FRET emission ratio (520/540 nm) observed between cells expressing interacting and noninteracting fusion proteins. Mean ratios calculated from indicated sample sizes. Error bars, standard deviation. Data adapted from Rajapakse et al.[53]

using recombinant proteins.[55] Maden Darby canine kidney (MDCKII) epithelial cells were transiently cotransfected with plasmid DNA encoding a C-terminal fusion of eDHFR to the PDZ1 domain (residues 19−113) of ZO-1 (ZO1-PDZ1/eDHFR) and an N-terminal fusion of EGFP to the C-terminal cytoplasmic domain (residues 187−211) of claudin-1 (GFP/cldn1-tail; see Figure 4a). We used osmotic lysis of pinosomes to load the otherwise membrane-impermeable **10** into the cytoplasm of transfected cells. Following intracellular delivery, time-gated FRET imaging revealed Tb-sensitized GFP emission only in transfected cells loaded with **10**, providing an unambiguous image of the protein−protein interaction (Figure 4b, top). By contrast, only faint FRET signals were seen in negative control cells that expressed a GFP/cldn1-tail construct lacking the C-terminal YV motif (GFP/cldn1-tail$^{\Delta YV}$), which is unable to bind to ZO-1, along with ZO-1/PDZ1-eDHFR (Figure 4b, bottom). Furthermore, there was a highly significant ($P < 10^{-6}$) >500% difference between the mean, donor-normalized FRET signal (520/540 nm emission ratio) from cells expressing ZO1-PDZ1/eDHFR and GFP/cldn1-tail and that seen from cells expressing noninteracting ZO1-PDZ1/eDHFR and GFP/cldn1-tail$^{\Delta YV}$ (Figure 4c).

The initial proof-of-principle study yielded three key results that support and guide our ongoing efforts to develop time-gated microscopy with lanthanides as a viable and, in some measures, improved alternative for live-cell FRET imaging. First, compound **10** diffuses freely throughout the cytoplasm and nucleus without detectable nonspecific binding and stably labels eDHFR. To our knowledge, this was the first reported example of selective, intracellular protein labeling with a lanthanide complex, and it suggests that other ligand/receptor tagging methods and improved forms of cytoplasmic probe delivery should prove equally useful. Second, **10** is sufficiently bright to enable single-channel TGD of intermolecular, Tb(III)-to-GFP-sensitized emission with image acquisition times of 1−4 s. These acquisition times are on the order of those seen with mutichannel, fluorescent protein-based, filter FRET measurements made on optimized microscopes;[24] further improvements may increase the time resolution of live-cell FRET imaging. Moreover, we observed that **10** remains stably luminescent in cells for hours and photobleaches with a lifetime of ∼2 min when excited with 365 nm light at the irradiance levels used on our system (∼0.5 mW/cm^2). Because typical exposure times are 1−4 s with the LED pulsing at 50% duty cycle, ∼30−100 images may be acquired before significant (>10%) photobleaching occurs. Third, elimination of background fluorescence allows FRET signals from positive (with interacting proteins) and negative (with noninteracting proteins) control cell samples to be distinguished with a high degree of confidence. Thus, lanthanide-based FRET may

dx.doi.org/10.1021/ic4018739 | Inorg. Chem. 2014, 53, 1839−1853

produce fewer false negative results in comparison to conventional FRET imaging techniques.

CELLULAR INTERNALIZATION AND LOCALIZATION OF LANTHANIDE COMPLEXES

Any *exogenous* luminescent probe or label intended for use in live-cell imaging experiments should ideally have the following properties: (i) the molecule should passively diffuse through lipid bilayers, thereby allowing delivery into the cell interior by the simple addition to a culture medium; (ii) the molecule should diffuse freely throughout all intracellular organelles and compartments, making it possible to study the widest range of biological phenomena; (iii) the molecule should not bind extensively or tightly to endogenous molecules, therefore allowing it to sense or interact with the target molecule of interest.[16,56] Delivery by passive diffusion makes it possible to control, to a certain extent, the overall amount of fluorophore that accumulates within the cells by varying the extracellular probe concentration and incubation time. If the probe does not bind appreciably to endogenous molecules, the cytoplasmic concentration will reach a steady-state level that never exceeds the extracellular concentration. Minimal levels of nonspecific binding are desirable because affinity for large macromolecules can sequester probes away from, say, target proteins or prevent diffusion into certain subcellular compartments.[56] For example, the nuclear pore complex allows passage of macromolecules <40 kDa; therefore, the binding of probes to large cytoplasmic proteins would prevent entry into the nucleus.[57] In practice, very few small-molecule fluorophores and, to our knowledge, no lanthanide complexes meet all of the aforementioned criteria.

The membrane permeability, intracellular distribution, and nonspecific affinity for endogenous biomolecules are dependent on the physicochemical properties including molecular size, charge, and lipophilicity. As with drug molecules, smaller, uncharged, and more lipophilic probes are more likely to be membrane-permeable.[58] Compounds with ionizable groups (e.g., carboxyl or sulfoxyl groups) are usually impermeant to cell membranes and only enter cells via facilitated diffusion through membrane channels or via endocytosis. Acylation of ionizable oxygen atoms and protection of carboxyl groups with esterase-labile acetoxymethyl or other esters are common strategies to make probes charge-neutral and thus enhance uptake kinetics.[48,59,60] Charge may also affect the intracellular distribution. Certain cationic dyes such as rhodamines partition to respiring mitochondria, which exhibit a negative potential across their inner membranes.[61] Anionic dyes such as fluorescein generally seem to exhibit less nonspecific binding and more even intracellular distribution. The apparent lack of intracellular, nonspecific binding seen with **10** may be due to its anionic character (net charge = −1) because most cytoplasmic proteins and DNA are anionic at physiological pH.[62]

Because lanthanide complexes are hydrophilic and often charged, they are unlikely to diffuse passively through lipid membranes. Therefore, effective intracellular delivery requires structural modifications that favor alternative uptake pathways (e.g., endocytosis) or experimental loading techniques that breach the plasma membrane. Direct microinjection of complexes into cells is a straightforward way to achieve cytoplasmic delivery,[63] but this method requires expensive apparatuses and considerable technical expertise. We have successfully adopted established biochemical methods of cytoplasmic delivery to enable intracellular protein labeling with the TMP−Lumi4 heterodimer **10**, including osmotic lysis of pinocytic vesicles[64] and reversible membrane permeabilization with the bacterial toxin streptolysin O.[65] While we showed that both loading techniques can be applied without compromising the cell viability,[53] their use requires careful optimization to achieve consistently uniform and high loading levels. Conjugation of lanthanide complexes to cell-surface receptor-targeting ligands or hydrophobic molecules has been shown to enhance cellular uptake. Bornhop and co-workers linked a cyclen-based chelator to PK11195, an isoquinoline carboxamide that binds selectively to the peripheral benzodiazepine receptor (PBR).[66] Cellular uptake and multimodal (MR and luminescence) imaging of C6 glioblastoma cells was achieved following the administration of a cocktail of PBR-targeted Eu(III) and Gd(III) complexes. The Meade group reported intracellular accumulation and progesterone-mediated transcription of a reporter gene following exposure of T47D breast cancer epithelial cells to progesterone−DOTA-Gd(III) conjugates.[67] More recently, Nagano and co-workers reported enhanced cellular uptake of DOTA-Gd(III) conjugated to hydrophobic dyes including Cy7 and boron dipyrromethene.[68]

Parker and co-workers have done extensive work to explore the effects of the probe structure on the cellular uptake and compartmentalization behavior of more than 60 cyclen-based Tb(III) and Eu(III) complexes.[69] The majority (∼80%) of compounds studied were microscopically observed to reside in endosomes or lysosomes following uptake into cells.[70] Similar cellular distributions were observed for helical, dinuclear Eu(III) complexes reported by Bunzli and co-workers.[71−73] Smaller subsets of Parker et al.'s compounds distributed in mitochondria,[74] or ribosomes and nucleoli.[75−77] From this series of work, it was found that the nature of the heteroaromatic sensitizing chromophore and its mode of attachment to the cyclen chelator, and *not* complex charge or lipophilicity, was the primary determinant of uptake kinetics and intracellular trafficking. Additional studies by Parker et al. showed substantial variation in the uptake kinetics, subcellular distribution, and cytotoxicity of 11 Tb(III) complexes variable only at a single position on the sensitizing chromophore.[39,78] These observations are consistent with follow-up studies that implicated macropinocytosis as the cell uptake mechanism for cyclen-based complexes.[79,80] Macropinocytosis involves nonspecific (i.e., receptor-independent) invagination and trapping of extracellular fluid and solutes within large (0.5−5 μm) cytoplasmic vesicles that subsequently fuse with endosomes or lysosomes.[81] Once taken into cells, probes may escape from inherently leaky macropinocytotic vesicles into the cytoplasm. There, they may be expected to traffic to cellular substructures in a manner dependent on their propensity to bind to endogenous membranes or biomolecules.

CELL-PENETRATING PEPTIDES (CPPS) FOR LANTHANIDE COMPLEX DELIVERY

Besides direct structural modification or conjugation to receptor-targeting ligands, covalent coupling to CPPs offers another means to effect enhanced cellular uptake of lanthanide complexes. CPPs are a class of short (10−30 amino acids), cationic peptides that have been shown in numerous studies to traverse biomembranes.[82−87] Considerable efforts have been made to characterize and optimize CPPs as molecular transporters that facilitate the passage of nucleic acids, proteins, therapeutics, and imaging agents into cells.[86,87] CPPs and their attached cargo can enter cells by two distinct routes:

dx.doi.org/10.1021/ic4018739 | Inorg. Chem. 2014, 53, 1839−1853

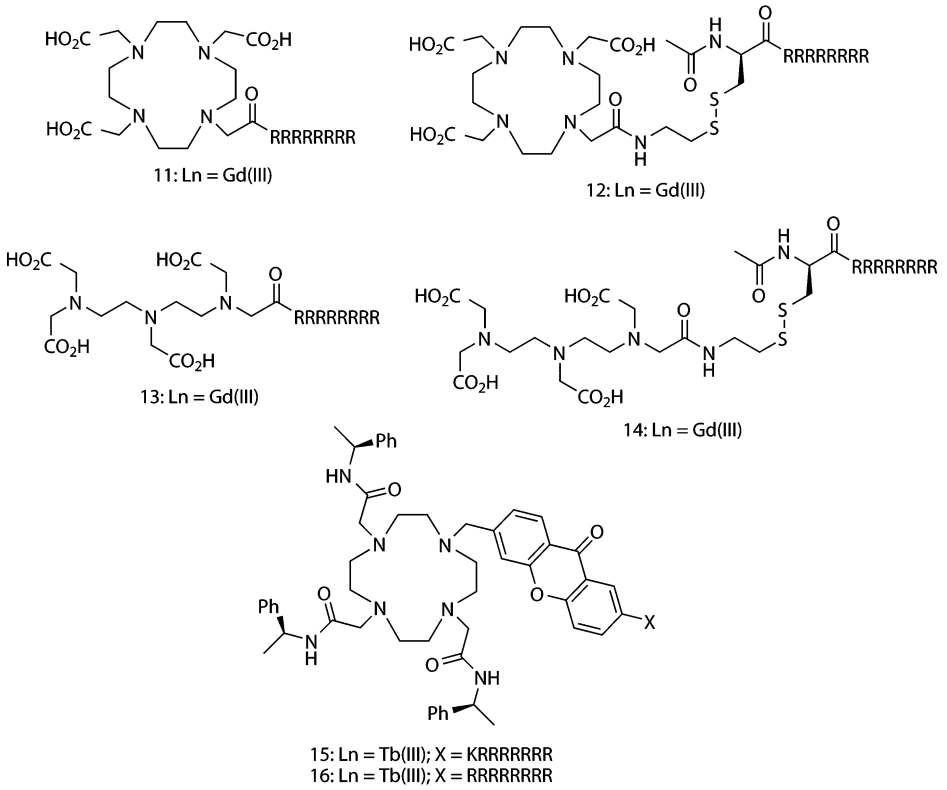

Figure 5. Reported lanthanide complexes conjugated to oligoarginine CPPs, which exhibit enhanced uptake into mammalian cells. Abbreviations: X = peptide sequence; capital letters, L-amino acids.

endocytosis and direct translocation through the lipid bilayer.[82−85] The extent to which either mechanism is operative depends on numerous factors including the CPP sequence, the size and type of cargo, the cell type, and the composition of the culture medium. Arginine-rich peptides such as oligoarginines or a fragment of the HIV-1 transactivating transcriptional activator (Tat, residues 49−57) are a class of CPPs that exhibit high transduction efficiency.[85] Studies using fluorophore-labeled oligoarginine and Tat reveal that these peptides utilize both endocytic and nonendocytic pathways. At lower micromolar concentrations, uptake has been observed to occur via macropinocytosis, clathrin-mediated endocytosis, and caveolae/lipid-raft-mediated endocytosis. However, above a threshold concentration (5−10 μM), uptake occurs via an energy-independent, nonendocytic pathway that leads to diffuse cytosolic and nuclear distribution of the peptides.[82−84]

CPPs have been covalently attached to lanthanide complexes to enhance cell uptake and retention (Figure 5). Both DOTA- and DTPA-Gd(III) chelates have been covalently linked to Tat and oligoarginine peptides to aid cell uptake.[88,89] Meade and co-workers have extensively explored oligoarginine as a delivery vehicle for MR contrast agents.[90−94] Conjugation to a peptide containing at least eight arginines, as shown for DOTA and DTPA analogues **11** and **13**, was found to be necessary for sufficient cell uptake.[91] Compounds **12** and **14**, which incoroporate a disulfide bond between DOTA-Gd(III) and DTPA-Gd(III) and octaarginine, exhibited enhanced retention in NIH/3T3 fibroblasts because the disulfide was cleaved in the reducing environment of the cell, presumably preventing peptide-mediated export.[93] Kielar et al. observed rapid (<5 min) internalization and endosomal localization of cyclen-based Tb(III) chelates that contained an N-coordinated, azaxanthone sensitizer conjugated to oligoarginines (compounds **15** and **16**).[39,78] A recent study by Thielemann et al. reported cellular uptake of pentadecanuclear Tb(III) and Eu(III) clusters linked to multiple CPP monomers. Confocal microscopy revealed distribution of the luminescent clusters within endosomes, cytoplasm, and the nucleus of HeLa cells, suggesting endocytosis and subsequent escape from endosomes/lysosomes as the mechansism of cell entry.[95]

We recently reported that covalent coupling to CPPs mediates cellular delivery of Lumi4-Tb and TMP−Lumi4 heterodimers and specific labeling of nucleus-localized eDHFR fusion proteins.[96] Several conjugates were prepared as N-terminal fusions of either Lumi4 or a heterodimer of Lumi4 and TMP to variations of nonaarginine (R_9) or Tat (Figure 6). We used TGD of Tb(III) luminescence or Tb(III)-mediated FRET signals to assess the cell uptake, subcellular peptide distribution, and specific intracellular protein labeling. For both Tat and R_9 conjugates, the mechanism of cell uptake and the resultant cellular distribution depended on the effective extracellular peptide concentration (Figure 7a). At low concentrations, Tb(III) conjugates enter cells via an endocytic pathway, resulting in a punctated cellular distribution. Above a threshold concentration, uptake occurs via direct translocation from the culture medium to cytoplasm, as evidenced by a diffuse distribution of Tb(III) luminescence throughout the cell. Incubation in a medium lacking fetal bovine serum (FBS) lowered the threshold concentration for observing diffuse staining (e.g., from 20 to 5 μM for **17**; Figure 7a) presumably because R_9 binds to serum proteins, thus lowering its effective concentration in the complete medium.[84] The observation of diffuse luminescence in MDCKII cells incubated at 4 °C in a serum-free medium containing **17** (10 μM) provided further

dx.doi.org/10.1021/ic4018739 | Inorg. Chem. 2014, 53, 1839−1853

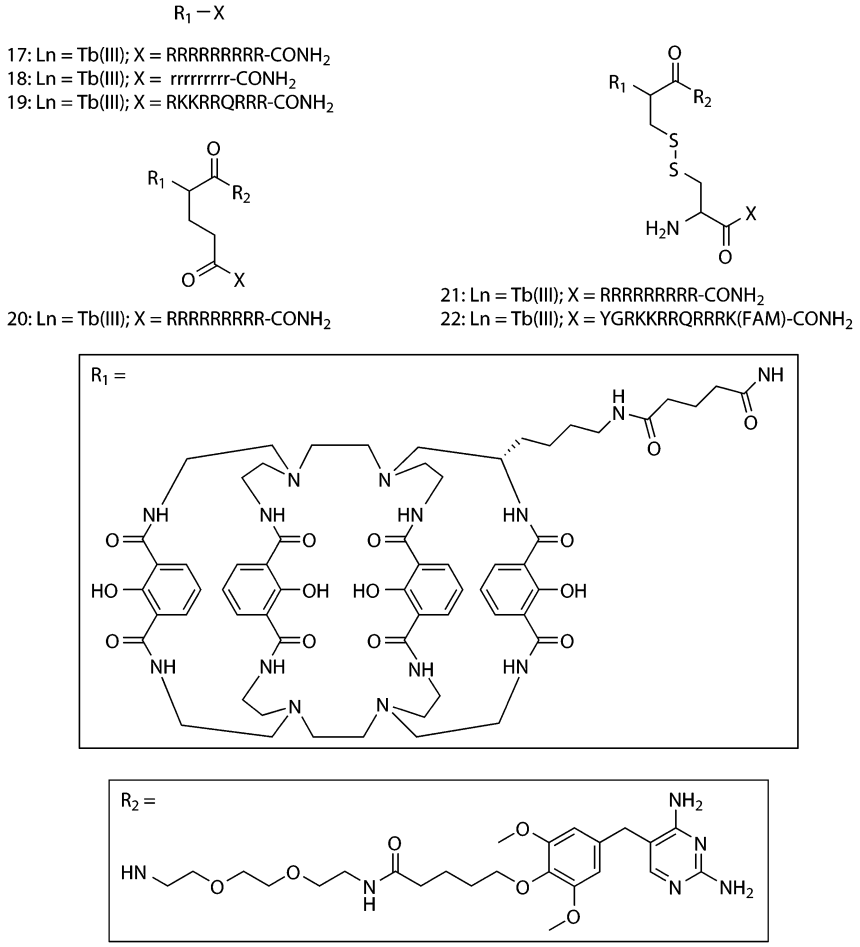

Figure 6. Structures of Lumi4−Tb(III) and TMP−Lumi4 heterodimers linked to nonaarginine- and Tat-derived CPPs. Abbreviations: R_1, linker-functionalized derivative of Lumi4; R_2, triethyleneglycolamino derivative of TMP; capital letters, L-amino acids; small letters, D-amino acids; FAM, 5,6-carboxyfluorescein.

evidence that uptake at higher effective concentrations occurs through an energy-independent, nonendocytic translocation mechanism (Figure 7a). We were able to identify experimental conditions that enabled the cytoplasmic delivery of all of the prepared conjugates into a variety of cell types including NIH/3T3, HeLa, and HEK293 cells.

Time-gated FRET imaging was used to directly visualize binding of CPP-conjugated, Lumi4−TMP heterodimers to an eDHFR fusion protein in live cells. We observed specific labeling of a three-component protein chimera consisting of histone 2B linked to the red fluorescent protein TagRFP-T[97] and eDHFR (H2B−TagRFPT−eDHFR). Following incubation of MDCKII cells in a medium containing **20**, time-gated imaging of Tb(III)-to-TagRFP-T-sensitized emission revealed nuclear luminescence that coincided with the steady-state fluorescence of TagRFP-T in expressing cells (Figure 7b). When unconjugated TMP was added to the imaging medium, it diffused into cells, competed with **20** for eDHFR binding, and eliminated the FRET signal (Figure 7b), providing further evidence of a direct interaction between **20** and H2B−TagRFPT−eDHFR. Similar results were seen with **21**, a cysteine amide-linked heterodimer of Lumi4 and TMP conjugated to CR_9 via a reducible disulfide bond. Intracellular reduction and cleavage of the disulfide bond was experimentally confirmed using compound **22**, a cysteine amide-linked heterodimer of Lumi4 and TMP via a disulfide bond to the Tat-derived peptide CYGRKKRRQRRRK(FAM). The intramolecular FRET signal between Tb(III) and a fluorescein moiety linked to the lysine side chain was observed to diminish within 30 min to 2 h following cell loading.

The ability to directly deliver protein-targeted Tb(III) complexes into the cytoplasm of live cells with technically simple, *mix-wash-image* experimental protocols will enable time-gated FRET imaging of a wide variety of target molecules. Furthermore, our results suggest that conjugation to the N-terminus of R_9 or Tat peptides via amide or disulfide linkages may offer a general strategy for the controlled cellular delivery of a wide variety of membrane-impermeable probes and protein labels. We are currently assessing the cell uptake performance of other R_9-linked probes including benzylguanine− and benzylcytosine−Lumi4−Tb(III) heterodimers that bind to SNAP and CLIP fusion proteins,[98] europium(III) poly(aminocarboxylate) complexes, and cyanine dyes. Additionally, we are working to quantify the extent to which the intracellular concentration of CPP conjugates can be controlled by varying the experimental labeling conditions.

QUANTITATIVE TIME-GATED MICROSCOPY WITH LANTHANIDES

The quality of fluorescence microscopic images, as indicated by perceived contrast, resolution, and SNR, is a function of the number of photons acquired by the imaging system.[99] Photon

dx.doi.org/10.1021/ic4018739 | Inorg. Chem. 2014, 53, 1839−1853

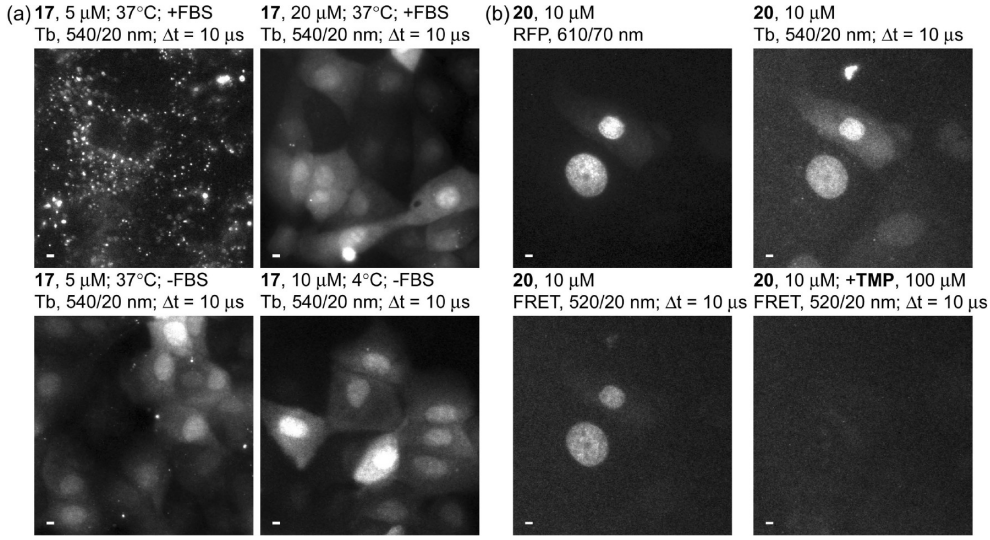

Figure 7. Arginine-rich CPPs conjugated to Lumi4−Tb(III) analogues directly translocating from a culture medium to cytoplasm and TMP−Lumi4−Tb(III) peptide conjugates binding to eDHFR following cytoplasmic delivery. (a) Micrographs of time-gated luminescence (delay = Δt = 10 μs, λ_{ex} = 365 nm, and λ_{em} = 540/20 nm). Scale bar, 5 μm. MDCKII cells were incubated for 30 min at the indicated temperatures in DMEM with (+) or without (−) FBS (10% v/v) that contained the indicated concentrations of **17**, a conjugate of Lumi4−Tb(III) to (L)-R_9. Incubation in DMEM with FBS containing a low (5 μM) concentration of **17** results in punctated Tb(III) luminescence (top, left), whereas incubation in DMEM with FBS above a threshold concentration (20 μM) results in the diffuse distribution of Tb(III) luminescence throughout the cytoplasm and nucleus (top, right). Incubation in DMEM without FBS lowers the threshold concentration (5 μM) for cytoplasmic delivery (bottom, left). Incubation at 4 °C results in a diffuse staining pattern (bottom, right), suggesting an energy-independent, direct-translocation uptake mechanism. (b) MDCKII cells transiently expressing H2B−TagRFPT−eDHFR incubated for 30 min at 37 °C in DMEM without FBS containing TMP−Lumi4−Tb(III) linked to the N-terminus of (L)-R_9 (**20**, 10 μM). A steady-state fluorescence (λ_{ex} = 545/30 nm and λ_{em} = 610/70 nm) image reveals nucleus-localized TagRFP-T fluorescence in expressing cells (top left). Time-gated images (delay = Δt = 10 μs, λ_{ex} = 365 nm, and λ_{em} as indicated) of Tb(III) luminescence (top, right) and Tb(III)-sensitized TagRFP-T emission (bottom, left) show that nucleus-localized FRET signals occur in expressing cells loaded with **20**. The sensitized emission signal disappears when TMP (final concentration = 100 μM) was added to the medium (bottom, right). Scale bar, 5 μm. Data adapted from Mohandessi et al.[96]

acquisition, in turn, depends on the microscope optics (magnification, NA, and transmittance), detector quantum efficiency, specimen properties (thickness and transparency), luminescent probe characteristics (brightness, lifetime, and concentration), and image acquisition parameters (excitation light intensity and exposure time). In practice, live cell imaging requires adequate photon acquisition from a limited number of fluorophores. For example, overexpressed fluorescent proteins and exogenous fluorescent sensors are typically imaged in mammalian cells at concentrations of 1−10 μM (10^6−10^7 copies per cell).[100,101] These cellular concentration levels reflect a need to balance detectability with minimal perturbation of the physiological function. Assuming a diffuse cytoplasmic distribution, a diffraction-limited volume element (∼1 fL) may contain only ∼100 fluorescent molecules. Furthermore, exposure times are limited by the need to resolve dynamic biological processes and to limit photobleaching of probes and photodamage to cells. Therefore, there is always a trade-off between the image quality and temporal resolution.

When imaging biosensors in living cells, the goal is often to measure, as precisely as possible, dynamic changes in the emission intensities over a range that reflects biochemically relevant changes in the biosensor activity (e.g., changes in the level of interaction between two proteins).[19] The precision of intensity measurements is characterized by SNR, which, for a Poissonian process, cannot exceed the square root of the number of photons/pixel in the image.[99] In practice, it is desirable to utilize the full dynamic range of a biosensor by imaging under conditions where the maximum emission intensity approaches detector saturation. The presence of background light from, for example, cellular autofluorescence increases the photon noise and reduces the effective capacity of the detector, thus reducing both the SNR and dynamic range. Maximal SNR is particularly important for filter FRET or ratiometric imaging where two or more raw images are processed postacquisition to quantify signal changes. When mathematical operations are performed on raw images, the stochastic noise adds to the total noise levels in the resulting ratio image.[31]

The ability to eliminate cellular autofluorescence and, for FRET imaging, directly excited acceptor fluorescence would seem to favor time-gated microscopy with lanthanide probes over steady-state fluorescence imaging with conventional organic fluorophores or fluorescent proteins. However, with long emission lifetimes and commensurately low photon emission rates, it is not clear whether the SNR achievable with lanthanides is high enough to quantitatively image biosensor activity under biologically relevant conditions. The Hahn laboratory is at the forefront of biosensor design and application, and their genetically encoded, FRET-based sensors of Rho-family GTPase activity represent a performance benchmark against which other sensor designs may be compared.[102,103] Hahn et al. have shown that single- and dual-chain biosensor activity can be quantitatively imaged in the cytoplasm of live cells at effective cellular concentrations of a few micromolars with exposure times of 0.3−0.9 s per image.[103] They used a filter-FRET-based approach, collecting two (for a single-chain sensor) or three (for a dual-chain sensor) images at successive time points, yielding total image acquisition times of up to several seconds on a microscope with motorized filter

dx.doi.org/10.1021/ic4018739 | Inorg. Chem. 2014, 53, 1839−1853

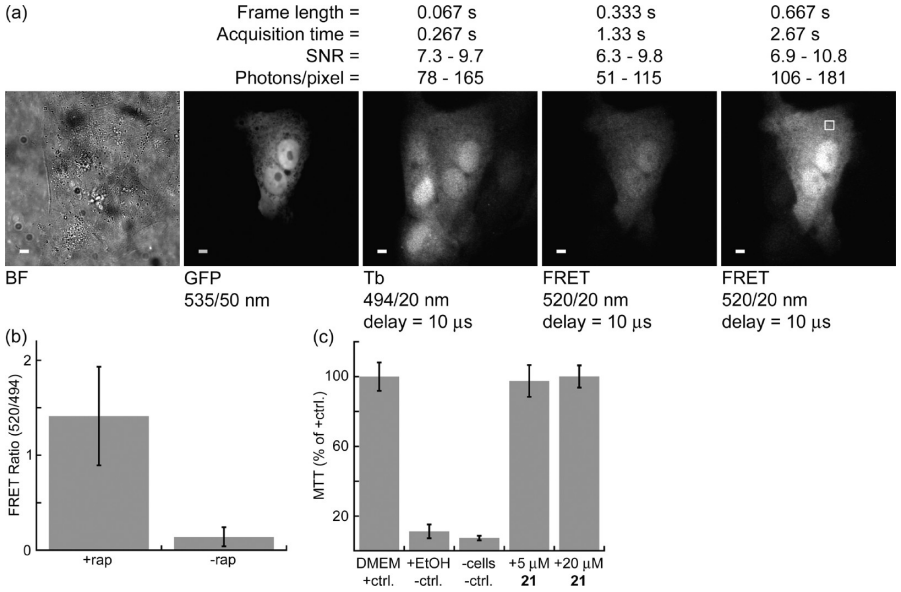

Figure 8. Interaction between GFP−FKBP12 and FRB−eDHFR imaged at high SNR. (a) MDCKII cells transiently coexpressing GFP−FKBP12 and FRB−eDHFR exposed to rapamycin (200 nM, 1 h) and subsequently incubated for 10 min at 37 °C in DMEM without serum containing **21** (7.5 μM), a Lumi4−CysTMP heterodimer linked via a disulfide bond to CR_9. The five images shown represent a single field of view acquired under different conditions: BF, bright field; GFP, steady-state fluorescence revealing the expressing cells; Tb, time-gated emission (494 nm) showing which cells were loaded with **21**; FRET, rightmost two images showing the Tb-to-GFP FRET signal observed in cells that both express fusion proteins and contain **21**. Time-gated Tb luminescence and FRET micrographs (delay = Δt = 10 μs, λ_{ex} = 365 nm, and λ_{em} as indicated) were generated by summing four frames of indicated length to yield single, 12-bit images. SNR and photons/pixel were calculated for a ROI in the cytoplasm (e.g., square in the rightmost image). The SNR was calculated as the mean background-subtracted pixel gray value in the ROI divided by its standard deviation. Values given are in the range for a 10-cell sample. FRET images are represented at identical contrast levels. Scale bar, 5 μm. (b) Bar chart representing the mean donor-normalized FRET emission ratio (520/540 nm) observed in FRET-positive (+rapamycin) and FRET-negative (−rapamycin) cells imaged at 0.667 s frame lengths. Error bars, standard deviation. (c) Relative MDCKII cell metabolic activity assessed with MTT assay. The bar chart shows the mean absorbance at 550 nm as a percentage of positive control (DMEM only) following incubation with **21** (30 min) at indicated concentrations (three replicates for each condition). Error bars, standard deviation.

changers. Each image typically has a SNR of at least 3 in the darkest regions. With these performance characteristics as a point of comparison, we have initiated studies to quantitatively assess lanthanide-based FRET imaging.

The rapamycin-induced interaction between FKBP12 and FRB[51,104] presents an ideal model system for quantifying the detection limit, SNR, dynamic range, and other measures of the image quality that may be observed with time-gated FRET imaging of protein−protein interactions. Because both proteins diffuse throughout the cytoplasm and nucleus when expressed in mammalian cells,[105] cytoplasmic signal levels are proportional to the total cellular protein concentration. Moreover, the degree of interaction can be controlled by titrating rapamycin levels, allowing for direct measurement of the FRET dynamic range. In a preliminary experiment, we transiently cotransfected MDCKII cells with DNA encoding GFP−FKBP12 and FRB−eDHFR. Following induction with rapamycin (200 nM, 1 h), cells were loaded with compound **21**, a cell-permeable conjugate of Lumi4−TMP linked to CR_9. Time-gated imaging revealed Tb(III)-to-GFP, FRET-sensitized emission only in expressing cells that were loaded with a probe (Figure 8a).

Time-gated FRET images were acquired at frame lengths of 0.333 and 0.667 s, and four frames were summed to increase the image SNR, yielding total acquisition times of 1.33 and 2.67 s, respectively. We measured the mean background-subtracted pixel gray values for regions of interest (ROIs) in the cytoplasm and calculated the GFP/Tb emission ratio, number of photons/pixel, and SNR (defined as the mean gray value divided by the standard deviation within the ROI) for a 9-cell sample. There was a highly significant (P = 0.0005), ∼10-fold difference between the mean cytoplasmic GFP/Tb emission ratio from FRET-positive cells imaged at 0.667 s frame lengths (+rapamycin, 1.4 ± 0.5) and FRET-negative cells (−rapamycin, 0.14 ± 0.10; mean ± standard deviation; Figure 8b). The mean number of photons/pixel observed in the cytoplasm ROIs ranged from ∼50−180 for Tb(III) luminescence and Tb-to-GFP FRET under the indicated imaging conditions, corresponding to SNRs of ∼6−11. An MTT assay was used to assess the MDCKII cell redox activity following exposure to **21**. No difference in the MTT reduction was observed in cells exposed to **21** (5 and 20 μM) for 30 min relative to that observed in positive control cells (Figure 8c), suggesting that CPP-linked Lumi4 analogues are nontoxic under typical exposure conditions used for these probes.

These results suggest that Tb(III)-mediated FRET microscopy can be used to quantitatively image protein−protein interactions in live cells. For accurate quantification of time-gated FRET signal changes, it should be sufficient to take a ratio of the FRET emission over the donor emission, necessitating only two images at each time point. Importantly, the SNR observed here exceeded the minimum value (5) considered acceptable for pixelwise, two-color ratiometric FRET imaging,[106] even at acquisition times of only ∼1.3 s. Two cameras can be mounted via a beamsplitter to simultaneously acquire FRET and donor images, thereby enabling single-frame imaging. Such an approach would improve temporal resolution in comparison to conventional filter FRET measurements, which require three images to

dx.doi.org/10.1021/ic4018739 | Inorg. Chem. 2014, 53, 1839−1853

accurately quantify bimolecular interactions. Further studies are underway in our laboratory using FKBP12/FRB and other model systems to quantify dynamic range and detection limits for time-gated FRET imaging. Because transient transfection yields widely varying expression levels of each fusion protein in different cells, we are preparing stable cell lines where GFP−FKBP12 is constitutively expressed at modest levels and FRB−eDHFR expression is under the control of an inducible promoter. Using this construct, we will be able to obtain statistically robust measurements of the image quality and relate these measurements to the total amount of protein expressed. We are also developing image analysis protocols that will allow for Tb(III)-mediated FRET quantification on a pixelwise basis, which is the standard for live-cell biosensor imaging.[103]

PHOTOTOXICITY OF UV EXCITATION LIGHT USED IN LANTHANIDE IMAGING

All Tb(III) complexes and most Eu(III) complexes with sufficient brightness and photostability for cellular imaging require near-UV (<380 nm) light for single-photon excitation. Because UV light is considerably more cytotoxic than visible or NIR radiation, lanthanide complexes have more limited applicability in live cells than conventional fluorophores. For chemists working in the field of lanthanide microscopy, it is helpful to understand the mechanisms of UV-mediated phototoxicity and the extent to which it poses a problem for live-cell studies. Such an understanding can guide the design of novel probes or experimental approaches that overcome phototoxicity limitations and expand the usefulness of lanthanide-based imaging methods.

Phototoxicity results from the production of reactive oxygen species (ROS) including superoxide ($^{\bullet}O_2^-$), hydroxyl radical ($HO^{\bullet}$), various peroxides, and, especially, singlet oxygen ($^1O_2$). ROS react with a variety of easily oxidizable cellular components, such as proteins, nucleic acids, and membrane lipids.[107] Native fluorescent species or exogenous fluorescent labels act as photosensitizers, reacting in their triplet excited state with dioxygen ($^3O_2$) to produce singlet oxygen ($^1O_2$). The magnitude of observed phototoxic effects then depends largely on the level of singlet oxygen production, which, in turn, depends on several variables including the concentration, subcellular location, and photochemical nature of sensitizing fluorophores, and the intensity and wavelength of the excitation light. For a given excitation intensity, UV light is more toxic than visible or NIR light because there are a variety of endogenous fluorescent species present in cells that can absorb UV light and sensitize ROS production, including flavins, NAD(P)H, and porphyrins.[108] For example, Gorgidze et al. observed wavelength-dependent mitotic inhibition in pig kidney embryo cells with near-UV (360 nm) light as 5 times more inhibitory than blue light (423−488 nm) and >50 times more inhibitory than green light (>500 nm).[109]

When the mechanism of UV-induced photodamage is orthogonal to the biological process being investigated or when UV exposure is limited, reliable experimental results can be obtained. For example, UV microscopy has been successfully used to image a number of cellular processes, including calcium signaling[110,111] and cholesterol distribution.[112] UV illumination is also commonly used for the photolytic activation of caged compounds.[113,114] Because our lanthanide imaging methodology requires only low exposures (~500 mW/cm^2) of short duration (1−3 s), it should be possible to obtain reliable results for many important cellular processes before damage accumulates, including cytoskeletal dynamics, golgi dynamics, or signaling molecule interactions that occur on time scales of seconds to a few minutes. As with any biological study, sufficient controls will be needed to ensure that experimental conditions do not affect the results. Moreover, oxygen scavengers (e.g., OxyFuor) or antioxidants such as ascorbic acid can be added to imaging media to minimize photodamage and prolong imaging experiments.[115] Therefore, lanthanide imaging with existing probe and microscope technologies should be immediately useful for a variety of biological applications.

Lanthanide probes that can be excited by visible light or by two-photon absorption in the NIR offer another means to overcome the limitations imposed by UV, single-photon excitation. A number of Eu(III) complexes with appreciable absorptivity at ~400 nm have been developed using acridone, coumarin, or azathiaxanthone as sensitizers.[76,116−118] The previously mentioned pentadecanuclear Eu(III) clusters reported by Thielemann et al. also absorb in this wavelength range.[95] Recent work by Maury and co-workers shows that push−pull, aryl−alkynyl chromophores can sensitize Eu(III) emission from a charge-transfer excited state, extending absorbance maxima well into the visible spectrum.[119] Such chromophores were recently used to develop very bright ($\varepsilon\phi_{em}$ > 30000 M^{-1} cm^{-1}), stable, triazacyclononaneeuropium(III) complexes,[120−122] albeit with shorter-wavelength absorption (λ_{max} = ~330 nm). Moreover, the charge-transfer character of the ligands can be tuned by varying donor substituents, allowing high two-photon excitation cross sections (>700 GM at 740 nm) and effective sensitization of Eu(III) luminescence.[123,124] At the present time, time-gated, multiphoton excitation with standard beam-scanning microscopies is likely to be impractical for live-cell imaging because of the long emission times of lanthanide complexes would require prohibitively long exposure times.[38] However, the ongoing development of fast-acquisition, two-photon microscopes,[125−127] coupled with the further development of multiphoton-excited lanthanide bioprobes opens up a new frontier for lanthanide-based cell imaging.

CONCLUSIONS AND FUTURE PERSPECTIVES

While TGD with millisecond-lifetime Tb(III) and Eu(III) lumiphores is firmly established for high-throughput screening and in vitro assays, the development of time-gated microscopy and lanthanide probe technologies for live-cell imaging has begun to accelerate. Increased understanding about the mechanisms by which lanthanide complexes interact with and enter cells will guide the future development of lanthanide sensors and protein labels. The ability to directly load luminescent Tb(III) complexes into the cytoplasm of live cells by conjugating them to CPPs and to selectively label intracellular fusion proteins (Figure 7) will enhance the development of lanthanide-based biosensors and time-gated FRET imaging of protein interactions and activity. The sensitivity of time-gated microscopes based on UV LED light sources and gated ICCD cameras makes it possible to image lanthanide luminescence and lanthanide-mediated FRET signals of protein−protein interactions at levels of protein expression and temporal resolution that are comparable to conventional fluorescence imaging (Figure 8). Further improvements in the probe design, CPP-mediated delivery, and quantitative time-gated microscopy will serve to make

dx.doi.org/10.1021/ic4018739 | Inorg. Chem. 2014, 53, 1839−1853

lanthanide-based imaging a routine tool for biological investigations.

EXPERIMENTAL SECTION

Materials and Reagents. Materials listed here and protocols given below pertain to data presented in Figure 8. Experimental methods for previously reported data (Figures 4 and 7) may be found in the cited references. Enzymes and cloning reagents were obtained from New England Biolabs, Inc. Cell culture reagents were purchased from Life Technologies, Inc. Plasmid vectors pRSETB−EGFP−FKBP12 and pRSETB−FRB−eDHFR were described previously.[51] MDCKII cells were obtained from the American Type Culture Collection (cat. no. CRL-2936). The synthesis and characterization of compound **21** was described in Mohandessi et al.[96]

Plasmids. A 318 bp fragment encoding FRB was amplified by PCR from pRSETB−FRB−eDHFR using the primers 5′-C GAC GCT CGA GAT AAG ATG CCA ATC CTC TGG C-3′ (*XhoI*, coding strand) and 5′-CC AGA TCC CGA ATT CAC CTT TGA GAT TCG TCG G-3′ (*Eco*RI, noncoding strand). This fragment was inserted between the *XhoI* and *Eco*RI sites in pLL-1 (Active Motif, Inc.) to generate pLL-1−FRB−eDHFR, encoding FRB−eDHFR. A 360 bp fragment encoding FKBP12 was amplified by PCR from pRSETB−EGFP−FKBP12 using the primers 5′-GGA AGT GCT CGA GGT GGA GTG CAG GTG G-3′ (*XhoI*, coding strand) and 5′-GCA GCC GGA TCC AGC TTC AGC TTA TTC CAG TTT TAG AAG C-3′ (*Bam*HI, noncoding strand). This fragment was inserted between the *XhoI* and *Bam*HI sites in pEGFP-C1 (Clontech, Inc.) to generate pEGFP−FKBP12, encoding GFP−FKBP12. The plasmid integrity was confirmed by direct sequencing.

Cell Culture, Transfection, and Labeling. MDCKII cells were cultured in Dulbecco's modified Eagle's medium (DMEM) supplemented with 10% fetal bovine serum (FBS), 2 mM L-glutamine, 100 unit/mL penicillin, and 100 μg/mL of streptomycin (DMEM+) at 37 °C and 5% CO_2. Cells were seeded at 10^5 cells per well into a 6-well plate. After ∼18 h of incubation at 37 °C and 5% CO_2, adherent cells (∼80% confluent) were cotransfected with 1 μg each of pLL-1−FRB−eDHFR and pEGFP−FKBP12 using Lipofectamine2000 (Invitrogen, Inc.) according to the manufacturer's instructions. Approximately 6 h after transfection, cells were trypsinized and reseeded at 15000 cells/well into 8-well-chambered coverglasses (Nunc, 12-565-470) and incubated at 37 °C and 5% CO_2 overnight.

Transfected cells growing in DMEM in 8-well-chambered coverglasses were washed once with phosphate-buffered saline (PBS), reimmersed in DMEM without FBS at 37 °C containing **21** (7.5 μM), and incubated for 10 min. Cells were washed 2 times in PBS and reimmersed in DMEM supplemented with 1 mM Patent Blue dye to quench extracellular luminescence of **21** bound nonspecifically to cells or coverslips. Following incubation and washing, cells were maintained (<1 h) at 37 °C and 5% CO_2 until imaging. The GFP−FKBP12/FRB−eDHFR interaction was induced by incubating cells in DMEM containing rapamycin (200 nM) at 37 °C for 1 h. Rapamycin induction was performed prior to loading the cells with **21**.

MTT Assay. The cellular metabolic activity following exposure to **21** was assessed using MTT (Life Technologies, cat. no. M6494) according to the manufacturer's instructions. MDCKII cells were seeded into clear-bottom, 96-well, tissue-culture-treated plates (30000 cells/well) and incubated in DMEM(+) at 37 °C and 5% CO_2 overnight. Cells were washed with 100 μL of PBS and reimmersed in a culture medium containing the following components (3 wells for each condition): positive control, DMEM(+) without phenol red (50 μL); negative control, EtOH (50 μL); DMEM(+) without phenol red containing 5 μM **21** (50 μL); DMEM(+) without phenol red containing 20 μM **21** (50 μL). Following 30 min of incubation at 37 °C and 5% CO_2, the cells were washed once with 100 μL of PBS and 100 μL of DMEM(+) without phenol red was added. MTT (1 μL of a 12 mM stock solution in PBS) was added to each well and mixed by pipetting. The cells were then incubated for 4 h at 37 °C and 5% CO_2. Then, 85 μL of medium was removed from each well and replaced with 50 μL of dimethyl sulfoxide (DMSO) to solubilize a MTT reduction product, the cells were incubated for 10 min, and the absorbance at 550 nm was measured on a plate reader (Perkin-Elmer, Victor 3 V). The absorbance of a second negative control consisting of DMEM(+) without phenol red (100 μL), MTT (10 μL), and DMSO (50 μL) was also measured. The mean absorbance (∼0.05 for negative control and ∼0.5 for positive control) for all conditions (three replicates) was plotted as a percentage of the absorbance measured for the positive control. Error bars represent the standard deviation.

Microscopy, Image Processing, and Analysis. Imaging of adherent live cells was performed using a previously described, modified epifluorescence microscope (Axiovert 200, Carl Zeiss, Inc.).[34] All images were acquired using a EC Plan Neofluar, 63×, 1.25 N.A. objective (Carl Zeiss, Inc.). Filter cubes containing the appropriate excitation and emission filters and dichroics allowed for wavelength selection. Continuous-wave fluorescence images were acquired using an Axiocam MRM CCD camera (Carl Zeiss, Inc.). For time-gated luminescence, pulsed excitation light from a UV LED (λ_{em} = 365 nm; illumination intensity = ∼0.5 W/cm^2 at the sample plane) was synchronized with the intensifier component of an ICCD camera (Mega-10EX, Stanford Photonics, Inc.) such that a 10 μs delay was inserted between the end of the LED pulse and the intensifier start time. For each acquisition, the signal from multiple excitation/emission events was accumulated on the ICCD sensor and read out at the end of the camera frame. The source/camera timing parameters and intensifier gain voltage settings were the same for all of the time-gated images and data presented: excitation pulse width = 1500 μs, pulse period = 3000 μs, delay time = 10 μs, intensifier on-time = 1390 μs, and gain = 778 V. The sensitivity of time-gated imaging is dependent on the number of excitation/detection events integrated on the CCD during a single camera frame and on the intensifier gain voltage. For frame lengths of 0.067, 0.333, and 0.667 s, the number of excitation/detection events equaled 22, 110, and 220, respectively. Frame summing was used to increase the SNR and to remove ion-feedback noise from the intensifier. Each frame summed effectively increases the bit depth of the resulting image in increments of 1024 (i.e., 1 frame yields a bit depth equal to 1024, 2 frames yield 2048, etc.). Images presented in Figure 8 are composites of four frames with a resulting bit depth of 4096.

ICCD images (tagged image file format, .TIFF) were captured with *Piper* control software (v2.4.05, Stanford Photonics, Inc.), and Axiocam images (.ZVI) were captured with Zeiss *AxioVision* software (v4.6). All images were cropped, adjusted for contrast, and analyzed using NIH *ImageJ* (v1.42q). For quantitative analysis of time-gated microscopic images, the emission signal intensity was calculated according to the equation $S = \mu_{signal} - \mu_{bckg}$, where μ_{signal} is equal to the mean pixel gray value in a region of interest (ROI) drawn within the cytoplasm and μ_{bckg} is equal to the mean pixel gray value in a similarly sized ROI in a nearby part of the image with no cells. The SNR was defined as S/σ_S, where $\sigma_S = (\sigma_{signal}^2 + \sigma_{bckg}^2)^{1/2}$. The mean number of photons/pixel was calculated from a proportionality factor that relates the pixel gray value to the apparent number of incident photons. The proportionality factor was measured from a graph of variance versus mean intensity for a set of images, as described in Gahlaut and Miller.[34] The donor-normalized FRET signal was defined as the ratio S_{520}/S_{540} of the mean gray values from the corresponding ROIs in each image pair. Cells were selected for analysis that exhibited both GFP expression and loading of **21** as determined by examination of the corresponding continuous-wave fluorescence images (λ_{ex} = 480/40 nm and λ_{em} = 535/50 nm) and time-resolved images of terbium emission (λ_{ex} = 365 nm and λ_{em} = 494/20 nm). The mean and standard deviation of FRET ratios was determined for a 10-cell sample each of cells expressing interacting (+rapamycin) and noninteracting (−rapamycin) fusion proteins. The *P* value was determined from a two-tailed, two-sample, unequal variance *t* test of each sample.

AUTHOR INFORMATION

Corresponding Author

*E-mail: lwm2006@uic.edu. Fax: 312 996 0431.

Notes

The authors declare no competing financial interest.

■ ACKNOWLEDGMENTS

We thank Dr. Darren Magda at Lumiphore, Inc., for ongoing material and intellectual support. This study was supported by the National Institutes of Health (National Institute of General Medical Sciences Grant R01GM081030-01A1) and by the National Science Foundation (Grant 1013776). Lumi4 is a trademark of Lumiphore, Inc.

■ REFERENCES

(1) Bunzli, J. C. *Chem. Rev.* **2010**, *110*, 2729−2755.
(2) New, E. J.; Parker, D.; Smith, D. G.; Walton, J. W. *Curr. Opin. Chem. Biol.* **2010**, *14*, 238−246.
(3) Ghose, S.; Trinquet, E.; Laget, M.; Bazin, H.; Mathis, G. *J. Alloys Compd.* **2008**, *451*, 35−37.
(4) Degorce, F.; Card, A.; Soh, S.; Trinquet, E.; Knapik, G. P.; Xie, B. *Curr. Chem. Genomics* **2009**, *3*, 22−32.
(5) Selvin, P. R. *Annu. Rev. Biophys. Biomol. Struct.* **2002**, *31*, 275−302.
(6) Hemmila, I.; Laitala, V. *J. Fluoresc.* **2005**, *15*, 529−542.
(7) Bunzli, J. C.; Eliseeva, S. V. Basics of lanthanide photophysics. In *Lanthanide luminescence: Photophysical, analytical and biological aspects*; Hanninen, P., Harma, H., Eds.; Springer- Verlag: Berlin, 2011; Vol. *7*, pp 1−47.
(8) Li, M.; Selvin, P. R. *J. Am. Chem. Soc.* **1995**, *117*, 8132−8138.
(9) Xu, J.; Corneillie, T. M.; Moore, E. G.; Law, G. L.; Butlin, N. G.; Raymond, K. N. *J. Am. Chem. Soc.* **2011**, *133*, 19900−19910.
(10) Hovinen, J.; Guy, P. M. *Bioconjugate Chem.* **2009**, *20*, 404−421.
(11) Terai, T.; Nagano, T. *Curr. Opin. Chem. Biol.* **2008**, *12*, 515−521.
(12) Nolan, E. M.; Lippard, S. J. *Acc. Chem. Res.* **2009**, *42*, 193−203.
(13) Chan, J.; Dodani, S. C.; Chang, C. J. *Nat. Chem.* **2012**, *4*, 973−984.
(14) Miller, L. W.; Cornish, V. W. *Curr. Opin. Chem. Biol.* **2005**, *9*, 56−61.
(15) Marks, K. M.; Nolan, G. P. *Nat. Methods* **2006**, *3*, 591−596.
(16) Jing, C.; Cornish, V. W. *Acc. Chem. Res.* **2011**, *44*, 784−792.
(17) Giepmans, B. N.; Adams, S. R.; Ellisman, M. H.; Tsien, R. Y. *Science* **2006**, *312*, 217−224.
(18) Xie, X. S.; Yu, J.; Yang, W. Y. *Science* **2006**, *312*, 228−230.
(19) Welch, C. M.; Elliott, H.; Danuser, G.; Hahn, K. M. *Nat. Rev. Mol. Cell Biol.* **2011**, *12*, 749−756.
(20) Zhang, J.; Campbell, R. E.; Ting, A. Y.; Tsien, R. Y. *Nat. Rev. Mol. Cell Biol.* **2002**, *3*, 906−918.
(21) Jares-Erijman, E. A.; Jovin, T. M. *Curr. Opin. Chem. Biol.* **2006**, *10*, 409−416.
(22) Miyawaki, A. *Annu. Rev. Biochem.* **2011**, *80*, 357−373.
(23) Jares-Erijman, E. A.; Jovin, T. M. *Nat. Biotechnol.* **2003**, *21*, 1387−1395.
(24) Piston, D. W.; Kremers, G. J. *Trends Biochem. Sci.* **2007**, *32*, 407−414.
(25) Sun, Y.; Day, R. N.; Periasamy, A. *Nat. Protoc.* **2011**, *6*, 1324−1340.
(26) Buranachai, C.; Kamiyama, D.; Chiba, A.; Williams, B. D.; Clegg, R. M. *J. Fluoresc.* **2008**, *18*, 929−942.
(27) Hum, J. M.; Siegel, A. P.; Pavalko, F. M.; Day, R. N. *Int. J. Mol. Sci.* **2012**, *13*, 14385−14400.
(28) Redford, G. I.; Clegg, R. M. *J. Fluoresc.* **2005**, *15*, 805−815.
(29) Colyer, R. A.; Lee, C.; Gratton, E. *Microsc. Res. Tech.* **2008**, *71*, 201−213.
(30) Hinde, E.; Digman, M. A.; Welch, C.; Hahn, K. M.; Gratton, E. *Microsc. Res. Tech.* **2012**, *75*, 271−281.
(31) Berney, C.; Danuser, G. *Biophys. J.* **2003**, *84*, 3992−4010.
(32) Galperin, E.; Verkhusha, V. V.; Sorkin, A. *Nat. Methods* **2004**, *1*, 209−217.
(33) Geissler, D.; Stufler, S.; Lohmannsroben, H. G.; Hildebrandt, N. *J. Am. Chem. Soc.* **2013**, *135*, 1102−1109.
(34) Gahlaut, N.; Miller, L. W. *Cytometry A* **2010**, *77*, 1113−1125.
(35) Beverloo, H. B.; van Schadewijk, A.; van Gelderen-Boele, S.; Tanke, H. J. *Cytometry* **1990**, *11*, 784−792.
(36) Seveus, L.; Vaisala, M.; Syrjanen, S.; Sandberg, M.; Kuusisto, A.; Harju, R.; Salo, J.; Hemmila, I.; Kojola, H.; Soini, E. *Cytometry* **1992**, *13*, 329−338.
(37) Connally, R. E.; Piper, J. A. *Ann. N.Y. Acad. Sci.* **2008**, *1130*, 106−116.
(38) Ramshesh, V. K.; Lemasters, J. J. *J. Biomed. Opt.* **2008**, *13*, 064001.
(39) Kielar, F.; Congreve, A.; Law, G. L.; New, E. J.; Parker, D.; Wong, K. L.; Castreno, P.; de Mendoza, J. *Chem. Commun. (Cambridge, U.K.)* **2008**, 2435−2437.
(40) Law, G. L.; Wong, K. L.; Man, C. W.; Wong, W. T.; Tsao, S. W.; Lam, M. H.; Lam, P. K. *J. Am. Chem. Soc.* **2008**, *130*, 3714−3715.
(41) Eliseeva, S. V.; Aubock, G.; van Mourik, F.; Cannizzo, A.; Song, B.; Deiters, E.; Chauvin, A. S.; Chergui, M.; Bunzli, J. C. *J. Phys. Chem. B* **2010**, *114*, 2932−2937.
(42) Vaasa, A.; Ligi, K.; Mohandessi, S.; Enkvist, E.; Uri, A.; Miller, L. W. *Chem. Commun. (Cambridge, U.K.)* **2012**, *48*, 8595−8597.
(43) Maurel, D.; Comps-Agrar, L.; Brock, C.; Rives, M. L.; Bourrier, E.; Ayoub, M. A.; Bazin, H.; Tinel, N.; Durroux, T.; Prezeau, L.; Trinquet, E.; Pin, J. P. *Nat. Methods* **2008**, *5*, 561−567.
(44) Doumazane, E.; Scholler, P.; Zwier, J. M.; Trinquet, E.; Rondard, P.; Pin, J. P. *FASEB J.* **2011**, *25*, 66−77.
(45) Strauch, R. C.; Mastarone, D. J.; Sukerkar, P. A.; Song, Y.; Ipsaro, J. J.; Meade, T. J. *J. Am. Chem. Soc.* **2011**, *133*, 16346−16349.
(46) Mizukami, S.; Yamamoto, T.; Yoshimura, A.; Watanabe, S.; Kikuchi, K. *Angew. Chem., Int. Ed.* **2011**, *50*, 8750−8752.
(47) Miller, L. W.; Cai, Y. F.; Sheetz, M. P.; Cornish, V. W. *Nat. Methods* **2005**, *2*, 255−257.
(48) Calloway, N. T.; Choob, M.; Sanz, A.; Sheetz, M. P.; Miller, L. W.; Cornish, V. W. *ChemBioChem* **2007**, *8*, 767−774.
(49) Rajapakse, H. E.; Reddy, D. R.; Mohandessi, S.; Butlin, N. G.; Miller, L. W. *Angew. Chem., Int. Ed.* **2009**, *48*, 4990−4992.
(50) Reddy, D. R.; Pedro Rosa, L. E.; Miller, L. W. *Bioconjugate Chem.* **2011**, *22*, 1402−1409.
(51) Yapici, E.; Reddy, D. R.; Miller, L. W. *ChemBioChem* **2012**, *13*, 553−558.
(52) Nguyen, A. W.; Daugherty, P. S. *Nat. Biotechnol.* **2005**, *23*, 355−360.
(53) Rajapakse, H. E.; Gahlaut, N.; Mohandessi, S.; Yu, D.; Turner, J. R.; Miller, L. W. *Proc. Natl. Acad. Sci. U. S. A.* **2010**, *107*, 13582−13587.
(54) Umeda, K.; Ikenouchi, J.; Katahira-Tayama, S.; Furuse, K.; Sasaki, H.; Nakayama, M.; Matsui, T.; Tsukita, S.; Furuse, M. *Cell* **2006**, *126*, 741−754.
(55) Itoh, M.; Furuse, M.; Morita, K.; Kubota, K.; Saitou, M.; Tsukita, S. *J. Cell. Biol.* **1999**, *147*, 1351−1363.
(56) Cunningham, C. W.; Mukhopadhyay, A.; Lushington, G. H.; Blagg, B. S.; Prisinzano, T. E.; Krise, J. P. *Mol. Pharmaceutics* **2010**, *7*, 1301−1310.
(57) Nigg, E. A. *Nature* **1997**, *386*, 779−787.
(58) Lipinski, C. A.; Lombardo, F.; Dominy, B. W.; Feeney, P. J. *Adv. Drug Delivery Rev.* **2001**, *46*, 3−26.
(59) Tsien, R. Y. *Nature* **1981**, *290*, 527−528.
(60) Minta, A.; Kao, J. P.; Tsien, R. Y. *J. Biol. Chem.* **1989**, *264*, 8171−8178.
(61) Baracca, A.; Sgarbi, G.; Solaini, G.; Lenaz, G. *Biochim. Biophys. Acta* **2003**, *1606*, 137−146.
(62) Schwartz, R.; Ting, C. S.; King, J. *Genome Res.* **2001**, *11*, 703−709.
(63) Hanaoka, K.; Kikuchi, K.; Kobayashi, S.; Nagano, T. *J. Am. Chem. Soc.* **2007**, *129*, 13502−13509.
(64) Okada, C. Y.; Rechsteiner, M. *Cell* **1982**, *29*, 33−41.

(65) Walev, I.; Bhakdi, S. C.; Hofmann, F.; Djonder, N.; Valeva, A.; Aktories, K.; Bhakdi, S. *Proc. Natl. Acad. Sci. U. S. A.* **2001**, *98*, 3185−3190.
(66) Manning, H. C.; Goebel, T.; Thompson, R. C.; Price, R. R.; Lee, H.; Bornhop, D. J. *Bioconjugate Chem.* **2004**, *15*, 1488−1495.
(67) Lee, J.; Burdette, J. E.; MacRenaris, K. W.; Mustafi, D.; Woodruff, T. K.; Meade, T. J. *Chem. Biol.* **2007**, *14*, 824−834.
(68) Yamane, T.; Hanaoka, K.; Muramatsu, Y.; Tamura, K.; Adachi, Y.; Miyashita, Y.; Hirata, Y.; Nagano, T. *Bioconjugate Chem.* **2011**, *22*, 2227−2236.
(69) Montgomery, C. P.; Murray, B. S.; New, E. J.; Pal, R.; Parker, D. *Acc. Chem. Res.* **2009**, *42*, 925−937.
(70) Frias, J. C.; Bobba, G.; Cann, M. J.; Hutchison, C. J.; Parker, D. *Org. Biomol. Chem.* **2003**, *1*, 905−917.
(71) Chauvin, A. S.; Comby, S.; Song, B.; Vandevyver, C. D.; Thomas, F.; Bunzli, J. C. *Chem.—Eur. J.* **2007**, *13*, 9515−9526.
(72) Chauvin, A. S.; Comby, S.; Song, B.; Vandevyver, C. D.; Bunzli, J. C. *Chem.—Eur. J.* **2008**, *14*, 1726−1739.
(73) Chauvin, A. S.; Thomas, F.; Song, B.; Vandevyver, C. D. B.; Bunzli, J. C. G. *Philos. Trans. R. Soc., A* **2013**, *371*, 20120295.
(74) Murray, B. S.; New, E. J.; Pal, R.; Parker, D. *Org. Biomol. Chem.* **2008**, *6*, 2085−2094.
(75) Yu, J.; Parker, D.; Pal, R.; Poole, R. A.; Cann, M. J. *J. Am. Chem. Soc.* **2006**, *128*, 2294−2299.
(76) Pal, R.; Parker, D. *Chem. Commun. (Cambridge, U.K.)* **2007**, 474−476.
(77) Pal, R.; Parker, D. *Org. Biomol. Chem.* **2008**, *6*, 1020−1033.
(78) Kielar, F.; Law, G. L.; New, E. J.; Parker, D. *Org. Biomol. Chem.* **2008**, *6*, 2256−2268.
(79) New, E. J.; Parker, D. *Org. Biomol. Chem.* **2009**, *7*, 851−855.
(80) New, E. J.; Congreve, A.; Parker, D. *Chem. Sci.* **2010**, *1*, 111−118.
(81) Falcone, S.; Cocucci, E.; Podini, P.; Kirchhausen, T.; Clementi, E.; Meldolesi, J. *J. Cell Sci.* **2006**, *119*, 4758−4769.
(82) Duchardt, F.; Fotin-Mleczek, M.; Schwarz, H.; Fischer, R.; Brock, R. *Traffic* **2007**, *8*, 848−866.
(83) Fretz, M. M.; Penning, N. A.; Al-Taei, S.; Futaki, S.; Takeuchi, T.; Nakase, I.; Storm, G.; Jones, A. T. *Biochem. J.* **2007**, *403*, 335−342.
(84) Kosuge, M.; Takeuchi, T.; Nakase, I.; Jones, A. T.; Futaki, S. *Bioconjugate Chem.* **2008**, *19*, 656−664.
(85) Nakase, I.; Takeuchi, T.; Tanaka, G.; Futaki, S. *Adv. Drug Delivery Rev.* **2008**, *60*, 598−607.
(86) Stewart, K. M.; Horton, K. L.; Kelley, S. O. *Org. Biomol. Chem.* **2008**, *6*, 2242−2255.
(87) Wender, P. A.; Galliher, W. C.; Goun, E. A.; Jones, L. R.; Pillow, T. H. *Adv. Drug Delivery Rev.* **2008**, *60*, 452−472.
(88) Bhorade, R.; Weissleder, R.; Nakakoshi, T.; Moore, A.; Tung, C. H. *Bioconjugate Chem.* **2000**, *11*, 301−305.
(89) Liu, M.; Guo, Y. M.; Wu, Q. F.; Yang, J. L.; Wang, P.; Wang, S. C.; Guo, X. J.; Qiang, Y. Q.; Duan, X. Y. *Biochem. Biophys. Res. Commun.* **2006**, *347*, 133−140.
(90) Allen, M. J.; Meade, T. J. *J. Biol. Inorg. Chem.* **2003**, *8*, 746−750.
(91) Allen, M. J.; MacRenaris, K. W.; Venkatasubramanian, P. N.; Meade, T. J. *Chem. Biol.* **2004**, *11*, 301−307.
(92) Endres, P. J.; Macrenaris, K. W.; Vogt, S.; Allen, M. J.; Meade, T. J. *Mol. Imaging* **2006**, *5*, 485−497.
(93) Endres, P. J.; MacRenaris, K. W.; Vogt, S.; Meade, T. J. *Bioconjugate Chem.* **2008**, *19*, 2049−2059.
(94) Major, J. L.; Meade, T. J. *Acc. Chem. Res.* **2009**, *42*, 893−903.
(95) Thielemann, D. T.; Wagner, A. T.; Rosch, E.; Kolmel, D. K.; Heck, J. G.; Rudat, B.; Neumaier, M.; Feldmann, C.; Schepers, U.; Brase, S.; Roesky, P. W. *J. Am. Chem. Soc.* **2013**, *135*, 7454−7457.
(96) Mohandessi, S.; Rajendran, M.; Magda, D.; Miller, L. W. *Chem.—Eur. J.* **2012**, *18*, 10825−10829.
(97) Shaner, N. C.; Lin, M. Z.; McKeown, M. R.; Steinbach, P. A.; Hazelwood, K. L.; Davidson, M. W.; Tsien, R. Y. *Nat. Methods* **2008**, *5*, 545−551.
(98) Gautier, A.; Juillerat, A.; Heinis, C.; Correa, I. R., Jr.; Kindermann, M.; Beaufils, F.; Johnsson, K. *Chem. Biol.* **2008**, *15*, 128−136.
(99) Murray, J. M.; Appleton, P. L.; Swedlow, J. R.; Waters, J. C. *J. Microsc.* **2007**, *228*, 390−405.
(100) Sala, F.; Hernandez-Cruz, A. *Biophys. J.* **1990**, *57*, 313−324.
(101) Tsien, R. Y. *Annu. Rev. Biochem.* **1998**, *67*, 509−544.
(102) Machacek, M.; Hodgson, L.; Welch, C.; Elliott, H.; Pertz, O.; Nalbant, P.; Abell, A.; Johnson, G. L.; Hahn, K. M.; Danuser, G. *Nature* **2009**, *461*, 99−103.
(103) Hodgson, L.; Shen, F.; Hahn, K. *Current Protocols in Cell Biology*; Wiley: New York, 2010; Chapter 14, pp 14.11.1−14.11.26.
(104) Brown, E. J.; Albers, M. W.; Shin, T. B.; Ichikawa, K.; Keith, C. T.; Lane, W. S.; Schreiber, S. L. *Nature* **1994**, *369*, 756−758.
(105) Inoue, T.; Heo, W. D.; Grimley, J. S.; Wandless, T. J.; Meyer, T. *Nat. Methods* **2005**, *2*, 415−418.
(106) Wang, Y. L. *J. Microsc.* **2007**, *228*, 123−131.
(107) Dailey, M.; Manders, E.; Soll, D.; Terasaki, M. Confocal Microscopy of Living Cells. In *Handbook of Biological Confocal Microscopy*; Pawley, J. B., Ed.; Springer: New York: 2006; pp 381−403.
(108) Konig, K.; Krasieva, T.; Bauer, E.; Fiedler, U.; Berns, M. W.; Tromberg, B. J.; Greulich, K. O. *J. Biomed. Opt.* **1996**, *1*, 217−222.
(109) Gorgidze, L. A.; Oshemkova, S. A.; Vorobjev, I. A. *Biosci. Rep.* **1998**, *18*, 215−224.
(110) Sako, Y.; Sekihata, A.; Yanagisawa, Y.; Yamamoto, M.; Shimada, Y.; Ozaki, K.; Kusumi, A. *J. Microsc.* **1997**, *185*, 9−20.
(111) Stricker, S. A.; Whitaker, M. *Microsc. Res. Tech.* **1999**, *46*, 356−369.
(112) Mukherjee, S.; Zha, X.; Tabas, I.; Maxfield, F. R. *Biophys. J.* **1998**, *75*, 1915−1925.
(113) Mitchison, T. J.; Sawin, K. E.; Theriot, J. A.; Gee, K.; Mallavarapu, A. *Methods Enzymol.* **1998**, *291*, 63−78.
(114) Ghosh, M.; Song, X.; Mouneimne, G.; Sidani, M.; Lawrence, D. S.; Condeelis, J. S. *Science* **2004**, *304*, 743−746.
(115) Knight, M. M.; Roberts, S. R.; Lee, D. A.; Bader, D. L. *Am. J. Physiol. Cell Physiol.* **2003**, *284*, C1083−C1089.
(116) Dadabhoy, A.; Faulkner, S.; Sammes, P. G. *J. Chem. Soc., Perkin Trans. 2* **2002**, 348−357.
(117) Bretonniere, Y.; Cann, M. J.; Parker, D.; Slater, R. *Org. Biomol. Chem.* **2004**, *2*, 1624−1632.
(118) Szijjarto, C.; Pershagen, E.; Ilchenko, N. O.; Borbas, K. E. *Chem.—Eur. J.* **2013**, *19*, 3099−3109.
(119) D'Aleo, A.; Picot, A.; Beeby, A.; Gareth Williams, J. A.; Le Guennic, B.; Andraud, C.; Maury, O. *Inorg. Chem.* **2008**, *47*, 10258−10268.
(120) Butler, S. J.; McMahon, B. K.; Pal, R.; Parker, D.; Walton, J. W. *Chem.—Eur. J.* **2013**, *19*, 9511−9517.
(121) McMahon, B. K.; Pal, R.; Parker, D. *Chem. Commun. (Cambridge, U.K.)* **2013**, *49*, 5363−5365.
(122) Walton, J. W.; Bourdolle, A.; Butler, S. J.; Soulie, M.; Delbianco, M.; McMahon, B. K.; Pal, R.; Puschmann, H.; Zwier, J. M.; Lamarque, L.; Maury, O.; Andraud, C.; Parker, D. *Chem. Commun. (Cambridge, U.K.)* **2013**, *49*, 1600−1602.
(123) D'Aleo, A.; Picot, A.; Baldeck, P. L.; Andraud, C.; Maury, O. *Inorg. Chem.* **2008**, *47*, 10269−10279.
(124) Picot, A.; D'Aleo, A.; Baldeck, P. L.; Grichine, A.; Duperray, A.; Andraud, C.; Maury, O. *J. Am. Chem. Soc.* **2008**, *130*, 1532−1533.
(125) Planchon, T. A.; Gao, L.; Milkie, D. E.; Davidson, M. W.; Galbraith, J. A.; Galbraith, C. G.; Betzig, E. *Nat. Methods* **2011**, *8*, 417−423.
(126) Truong, T. V.; Supatto, W.; Koos, D. S.; Choi, J. M.; Fraser, S. E. *Nat. Methods* **2011**, *8*, 757−760.
(127) Choi, H.; Tzeranis, D. S.; Cha, J. W.; Clemenceau, P.; de Jong, S. J. G.; van Geest, L. K.; Moon, J. H.; Yannas, I. V.; So, P. T. C. *Opt. Express* **2012**, *20*, 26219−26235.